Final Technical Report
for Grant NAG 5-298

CONSTRAINTS ON LITHOSPHERIC STRUCTURE FROM
SATELLITE POTENTIAL FIELD DATA:
AFRICA AND ASIA

March 1, 1983 through May 31, 1985

MAR 1986
RECEIVED
NASA STI FACILITY
ACCESS DEPT.

ANALYSIS AND INTERPRETATION OF MAGSAT
ANOMALIES OVER NORTH AFRICA

Southern Methodist University
Dallas, Texas 75275
for
Department of Geological Sciences

Roger J. Phillips
Principal Investigator

ABSTRACT

Crustal anomaly detection with Magsat data is frustrated by the inherent resolving power of the data and by contamination from the external and core fields. The quality of the data might be tested by modeling specific tectonic features which produce anomalies that fall within the proposed resolution and crustal amplitude capabilities of the Magsat fields. To test this hypothesis, the north African hotspots associated with Ahaggar, Tibesti and Darfur have been modeled as magnetic induction anomalies due solely to shallower depth to the Curie isotherm surface beneath these features.

The magsat data were reduced by subtracting the external and core fields to isolate the scalar and vertical component crustal signals. Of the three volcanic areas, only the Ahaggar region had an associated anomaly of magnitude above the error limits of the data. The goal then became to test the hotspot hypothesis for Ahaggar by seeing if the predicted magnetic signal matched the Magsat anomaly.

The predicted model magnetic signal arising from the surface topography of the uplift and the Curie isotherm surface was calculated at Magsat altitudes by the Fourier transform technique of Parker (1972) modified to allow for variable magnetization. The Curie isotherm surface was calculated using a method discussed by Birch (1975) for the temperature distribution in a moving plate above a fixed hotspot. The magnetic signal was calculated for a fixed plate (i.e., velocity set at zero) as well as a number of plate velocities and directions.

This study recognized several difficulties with the Magsat data, including: 1) the vertical component data are severely effected by the

spacecraft attitude uncertainties seen as a phase shift in the anomaly signals, 2) the necessity of using map formats of the Magsat data for correlation with known tectonic features and 3) the effects of the external current system on the crustal signal. Despite these limitations on the quality of the data, model/data correlations were found. In summary it is suggested that the region beneath Ahaggar is associated with a strong thermal anomaly and the predicted anomaly best fits the associated Magsat anomaly if the African plate is moving in a northeasterly direction.

TABLE OF CONTENTS

LIST OF FIGURES

LIST OF TABLES

CHAPTER 1

INTRODUCTION

The Magsat (magnetic satellite) mission had several scientific objectives including 1) testing core field models, 2) isolation of crustal fields for anomaly interpretation and 3) investigations of fields from the external current system. The crustal field mapping involved aquisition of data for regional studies of the induced and remanent magnetization of the lithosphere. Because this mission is relatively recent, the accuracy and resolution of this data set in detecting all but the most robust of the crustal anomalies is not well established. One test of the utility of the Magsat data would be to model tectonic features that produce anomalies that should in principle be large enough to detect at satellite altitudes. The Ahaggar, Tibesti and Darfur volcanic regions of north central Africa (figure 1) were selected in this study for evaluating the Magsat crustal data set.

In recent years, there has been increased interest in the tectonic evolution of the African plate. This plate has one of the slowest velocities (Gass,1978) as well as a large amount of intra-plate volcanism and other active geologic

features. The intra-plate volcanism is thought to be the result of mantle heat sources or hotspots (Burke and Wilson,1972).

The objective of this research is twofold. First, it is to study and thermally model the north central African lithosphere. Secondly, the results will be compared with measured Magsat anomalies. The lithosphere model that is to be generated will be based on the hotspot hypothesis that holds that there are relatively fixed localized regions of upwelling heat from the mantle (Morgan,1972) and the concept of simple thermal isostasy. The hotspot evaluation leads to lithospheric thinning and uplift due to heating from the mantle heat source (Detrick and Crough,1978). The magnetic model will be calculated using an extension of a Fourier transform technique developed by Parker (1972) for determining the magnetic signature due to an uneven layer of material. The base of this layer will be the Curie isotherm surface below which material looses its magnetic properties. Long wavelength magnetic anomalies should be directly related to positioning of this isotherm below the surface.

The Magsat data used for this research were reduced to the vertical and scalar components following a method similar to that used for the derivation of the published Magsat maps (Langel et al., 1982a,1982b). The component data were contoured and plotted with separate maps for the ascending and descending orbits. Recent work on the Magsat data has uncovered noise errors inherent within the

different data sets (Maeda et al., 1982) and so this subdivision of the data into ascending and descending orbits was used to isolate the noise components.

Investigation of the proposed magnetic models will be limited by the error sources in both the model and magnetic data. Spacecraft attitude uncertainties, instrument error, effects of external currents as well as reduction techniques limit the quality of the Magsat data and the magnetic model is burdened by the assumption that most of the physical parameters of the magnetic layer are constant.

It is therefore the purpose of this research to devise a magnetic model for the three hotspots of north Africa by mapping variations of the Curie isotherm surface that best fit the associated Magsat magnetic vertical and scalar anomalies. Through this analysis, it is hoped that a better understanding of the resolution of the Magsat data in detecting crustal signals as well as the tectonic significance of these volcanic areas will be gained.

CHAPTER 2

BACKGROUND DISCUSSION

2.1 Introduction

Africa has experienced a complex geologic history. The imprint of a number of Precambrian orogenic events can be distinguished in the cratonic regions. From the Precambrian to the present, episodes of magmatic activity have affected the entire continent. The African plate is still very active with an extensive rift system and scattered intra-plate volcanic regions.

Piecing together this complicated history has been difficult for researchers because of the inacessibility of most of Africa. The East African rift system has attracted considerable interest, but areas such as the north central Africa still have only sparse field data. The limited amount of data has resulted in modeling of only small scale tectonic features, and descrepancies exist for the overall tectonic framework. The motion of the African plate is presently in dispute. From the Jurassic rifting of Africa from South America to the present day, gaps in this time sequence have yet to be explained. It is an encumbering

problem to solve with the diverse nature of the present day plate boundaries.

In this section, I review the tectonic evolution of the African plate for the past 25 Ma and the geology and geophysics of the specific regions of north Africa for which I have conducted Magsat studies.

2.2 Geologic Setting

The volcanic regions to be studied and modeled are the Ahaggar, Tibesti and Darfur uplifts (figure 2), three topographically distinct areas in North Africa. These volcanic provinces are located in the Sahara Desert region surrounding the Chad Basin and flanked to the north by the Murzuk and Kufra Basins. This area was affected by the 650 Ma Pan-African orogenic event, has been the site of extensive Paleozoic to Tertiary sediment deposition, and has experienced uplift with associated alkaline volcanism during the past 25 Ma. During this last time period, the structural and geologic histories of these three areas exhibit some similarities, but prior to the Cenozoic volcanism their tectonic evolutions are somewhat distinct.

Of the three, Ahaggar has the greatest surface exposure of Precambrian basement. This province covers an area roughly 700 x 1000 kilometers and reaches an elevation close to 3 kilometers. The exposed basement shows a complex history of four Precambrian orogenic events (Crough,1981b) the latest being the Pan-African. These tectonic events can be distinguished by the major north-south trending faults

(Black and Girod,1970). Paleozoic alkaline intrusives occur in the eastern and southern regions of the massif, but this time period was for the most part a magmatically quiet one. The areas surrounding the massif were subjected to transgressive-regressive deposition. During the Cretaceous, granitic ring complexes developed, and there was an increase in continental sedimentation with Cretaceous sediments resting unconformably on the basement. This activity may imply a rejuventation of the basement (Black and Girod,1970).

In north Africa, tholeiitic volcanism is restricted to the west African craton during periods of downwarping, but the Recent alkaline volcanism and younger alkali granites tend to occupy zones of uplift and pre-existing transcurrent faults (Black and Girod,1970). This Recent volcanism formed strato-volcanoes of the strombolian type overlying Precambrian metamorphic basement. The timing of the Recent epierogenic activity is not well documentated. It is thought that around Pliocene time the Ahaggar Massif and the Air Massif to the south were uplifted (Black and Girod,1970). The present day NNW compressive stress directions correlate with the present-day plate convergence between Africa and Eurasia (Yee-han Ng,1983).

In contrast to Ahaggar, the Tibesti Massif covers an area 350 x 500 kilometers, but also reaches elevations of over 3 kilometers. The high volcanic peaks lie on a Precambrian metamorphic basement elevated to 2 kilometers

(Vincent,1970). The Precambrian tectonic evolution of this region is not as complex as Ahaggar, having only two distinct tectonic units separated by an unconformity (Vincent,1970). The basement rocks are overlapped by an unconformable Paleozoic sedimentary cover. During the Paleozoic, the region experienced its maximum uplift along northeast trending faults following the Precambrian trends (Vincent,1970). After deposition of the Cretaceous Nubian sandstone, the massif was cut into sections by northeast and north-northeast trending faults also following the Precambrian trends (Vincent,1970). The Tertiary to Recent history of this region was a period of intense igneous activity with flood basalts and the formation of shield volcanoes. The dominant composition of the volcanic rocks is alkaline. The Tibesti massif is still currently experiencing geothermal activity.

Of the three regions, Darfur has had the least complicated tectonic history. The major structural trends are north-south to north-northwest and the basement rocks were highly folded and metamorphosed during the Pan-African event. Darfur is comprised of three volcanic regions with a total surface area roughly 200 x 300 kilometers overlying a broad uplift 500-1000 meters in height extending from the Chad Basin in the west to the Nile Basin in the east. The Jebel Marra volcanic complex is the most extensive and forms the topographic highest region in this area. The Precambrian gneisses and schists of Darfur were buried by a thick cover of Cretaceous Nubian sandstone and subsequently

uplifted during the Tertiary (Francis et al.,1973). Paleozoic granites emplacement, quartz veins and dykes cut across the northeast - southwest foliation of the gneisses (Vail,1978). Recent igneous activity included the eruption of both ignimbrites and basaltic lavas in the form of flows, plugs, vents and craters widespread over the uplift. The most prominent feature of Darfur is the caldera in the Jebel Marra complex, which reaches an elevation of 3 kilometers. The caldera containing a recent pyroclastic cone, is considered dormant, but presently experiences geothermal activity. Carbonized wood within a major eruption was dated using Carbon-14 techniques at 3,520+100 years and the basal lavas at Jebel Marra have been dated at approximately 13.5 Ma (Bermingham et al.,1983). Volcanic activity occurred in two phases with the first being alkaline in composition. This phase was followed by erosion and deposition of alluvial material. The second phase was a basalt-trachyte association in a variety of flow types.

2.3 Geophysical Studies

Geophysical interpretations of north Africa have been limited because of lack of available data. The surface data for this area consist of Bouguer gravity measurements in the Darfur region, seismic data from areas near the Ahaggar uplift and limited Free-air gravity data for Darfur and Ahaggar. Despite the limitations of the data, a few authors

have presented geophysical models for these three uplifts and attempted to fit their evolution into a larger tectonic framework.

The surface gravity data for Darfur consists of one east-west traverse across the uplift taken during an expedition in 1975 (Brown and Girdler,1980a). Using very limited gravity and published topographic data, a predicted Bouguer gravity map for Africa was compiled (Brown and Girdler, 1980b). From this predicted map, a negative 60 mgal Bouguer anomaly is seen to coincide with the high ground linking the uplifted Ahaggar, Tibesti and Darfur areas (Fairhead, 1980) (figure 3). The gravity anomaly extends WNW-ESE and is not a part of the larger negative anomaly associated with the East African rift. The areal exent of the low density volcanics is smaller than the gravity anomaly, suggesting that deeper sources must contribute to this mass deficiency (Brown and Girdler, 1980b).

Brown and Girdler (1980b) calculated crustal models for the uplifted areas using the predicted gravity data and related the negative anomaly to a thinning of the lithosphere. Their model predicts that the lithosphere thins to approximately 60 kilometers under the topographic highs. They explain this phenomenon by lateral forces acting on the lithosphere, causing it to fracture, where upon intrusion of magma leads to thermal expansion and thinning.

Bermingham et al. (1983) using the gravity data taken along the Darfur traverse, modeled the Jebel Marra volcanic complex. A long wavelength negative regional anomaly with

an amplitude of 20 mgals is centered over the entire swell and extends approximately 2000 kilometers from Lake Chad to the White Nile. Superimposed on this anomaly is a negative 50 mgal anomaly 500 kilometers wide situated across the Darfur dome. After a negative 60 mgal regional anomaly was removed, four models were calulated from the residual anomaly. Two of the models were consistent with teleseismic delay times, which imply low density material within the lithosphere. One model is a laccolith in the upper part of the lithosphere and the other model is a lithosphere thinned to 50-60 kilometers. Both models assume a negative .05 grams/cubic centimeter density contrast.

Brown and Fairhead (1983) and Bermingham et al. (1983) interpret the Darfur dome as an unfractured third arm of a continental triple junction. The other two arms are the Ngaoundere rift trending WSW from Darfur to the Cameroons and the Abu Gabra rift trending southeast from Darfur to the East African rift. They call this the Central African rift system and believe that it is presently at the mid-Miocene stage of the East African rift (broad domal uplifts and volcanism in the form of flows). If their hypothesis is correct, then the Central African rift should presently be forming a more extensive fracture system.

Using POGO (Polar Orbiting Geophysical Observatories) magnetic satellite and surface gravity data, Jain and Regan (1982) modeled the eastern and western rift valleys. Despite the limited resolution of the magnetic data due to the high

altitudes of the satellite (400-1510 kilometers), small anomalies (less than 3 gammas) are seen across the rift valleys. They presented a magnetic model showing a rise in the Curie isotherm from 35 kilometers (assuming the MOHO is the magnetic boundry) to 19 kilometers and a thinning of the lithosphere from 100 kilometers to 84 kilometers. The gravity model using a crustal density of 2.88 grams/cubic centimeter and asthenospheric density of 3.22 gm/cm^3 shows a thinning of the lithosphere to 50-60 kilometers. This range of thinning is consistent with that found for oceanic swells (Crough,1978).

Crough (1981a,1981b) used Free-air gravity data to calculate isostatic models for the Ahaggar and Darfur uplifts (figure 4a,4b). The data show only a small positive Free-air anomaly, suggesting isostatic equilibrium of the uplift. His model assumes a uniform density crust and that Free-air gravity over swells is proportional to isostatic root depth. Crough calculated a root depth or depth of compensation between 40-70 kilometers for Darfur (Crough,1981a) and 60 kilometers for Ahaggar (Crough,1981b). He argued that the thinning is due to magma production within the asthenosphere, which causes thermal expansion and hence a density decrease in the lithosphere. The methods Crough (1981a,1981b) used for modeling the swells will be discussed in a later section and used as a starting point for the thermal models presented in this study.

2.4 Tectonic Evolution

Structurally, Africa contains three cratonic regions which typically have lower mean elevations than the continental averages, lower heat flow than the non-cratonic areas and a cratonic lithosphere thickness thought to exceed 200 kilometers (Gass,1978), and to have been unaffected by regional tectono-thermal events during the last 1100 Ma. The non-cratonic regions have elevations near or above the continental mean with a basin and swell topography (Burke and Wilson,1972;Gass,1978). These areas were affected by the 650 Ma Pan-African thermal event and have had extensive volcanism during the last 25 Ma.

Briden and Gass (1974) have attempted to fit African magmatism into a tectonic framework, and found that the last three major African igneous and metamorphic episodes coincide with pauses in the motion of the African plate. These episodes occurred 650-400 Ma, 200-100 Ma and 25 Ma to present. The earliest of these three episodes is the Pan-African event which produced regional metamorphism and reactivation of older basement throughout most of the African plate. The Mesozoic activity is confined to South Africa and a small area in Northeast Africa and is not as well defined a magmatic period as the other two. Briden and Gass (1974) based their tectonic-magmatic correlations on apparent polar wandering paths for Africa. During the three magmatic periods, they found no motion of the pole and

concluded that it reflects episodes of non-movement of the African plate.

Duncan (1981) studied the large number of hotspot traces on the African plate (figure 5). Many of these have been active since the Cretaceous. The Prince Edward Island, Bouvet, Tristan da Cunha and St. Helena are the longest continuous traces. Using available geochronological data, Duncan determined rotation poles for Africa. For other suspected hotspots with less obvious traces he superimposed the rotation pattern and determined the trends. The trends do not appear to fit for all the hotspots, and this lack of correlation could result from failure to consider the effects of the East African rift system. Some authors have questioned the validity of hotspots as absolute reference frames. Burke et al. (1973) examined the Atlantic hotspots using the Colorado seamount as a fixed reference point. They found that hotspots do migrate, but in small groups (e.g. Atlantic hotspots) remain fixed. Duncan concluded that for short time periods hotspots can be considered stationary with respect to the underlying mantle.

The past 25 Ma of the tectonic history of Africa is marked by intense intra-plate volcanism and rifting. This recent surge of alkaline volcanism is scattered throughout north central and northwest Africa with the most extensive volcanic fields centering along the East African rift system. The African plate has not been subjected to any orogenic activity during this period, so the increase in magmatic activity results from thermal plumes or hotspots

within the mantle (Gass,1978). Burke and Wilson (1972) believe that this sudden increase in volcanic activity results from the termination of movement of the African plate at 25 Ma. If the African plate has had static periods, a mantle thermal source would be concentrated at the base of the plate to a much higher degree. Burke and Wilson (1972) and Briden and Gass (1974) use this as evidence for a motionless plate because it explains the increase in magmatic activity. Other lines of evidence presented by Burke and Wilson (1972) are the altered motion of spreading in the Indian Ocean 21 Ma ago and the termination of the Tristan da Cunha and Gough aseismic ridges east of magnetic anomaly six (25 Ma). Other seamount chains in the Atlantic are thought to lie west of the ridgecrest (e.g. Discovery and Meteor). One problem with the theory is the lack of Recent volcanism on the cratonic regions. The two previous magmatic episodes had extensive cratonic activity. It is entirely possible that 25 Ma is too short a time period for a thermal source to effect a thick, stable cratonic area in the absence of pre-existing zones of weakness. However, in support of this theory, the extensive intra-plate or hotspot volcanism in the non-cratonic areas does not show the typical hotspot traces evident in moving plates. Contradicting the theory that there is absolutely no plate motion are studies done by Chase (1978), McKenzie and Sclater (1971) and Duncan (1981).

Chase (1978) inverted all the reliable data available

(e.g. seafloor spreading rates, transform fault trends and earthquake slip vectors) for the motion of twelve major plates. He calculated Euler poles and vectors and estimated from these a northeast rotation of Africa of .5 centimeters/year near the rotation pole in west Africa to 2 centimeters/year at the southern boundary of the plate. McKenzie and Sclater (1971) studied magnetic seafloor anomalies and transform fault trends in and around the Indian Ocean. They calculated a northeast movement of Africa at 2 centimeters/year relative to Antartica in the southwest Indian Ocean. Duncan (1981) using geochronological data from some of the aseismic ridges and hotspot reference frames showed a continous northeast migration of the African plate for the past 25 Ma. For hotspots where age dates are not available such as those in the north-central region, Duncan interpolated the hotspot trace in terms of the relative plate motion. Duncan's conclusions are speculative because if the African plate is moving with a slow velocity any hotspot formed 25 Ma might not show a very distinct surface trend.

From this brief summary of the previous work on the tectonic evolution of the African plate, it is apparent that the Recent history has been complex. The development of an extensive rift system as well as the scattered intra-plate volcanism seem to be related to the African plate being subjected to a number of stresses. It is the hope that this present research involving a closer look at the intra-plate volcanic areas would provide additional information to

better clarify this complex history.

CHAPTER 3

MAGSAT DATA

3.1 Introduction

In October of 1979, the Magsat satellite was put into a twilight, sunsynchronous orbit along the dawn-dusk meridian for a mission which lasted approximately seven and one-half months. The purpose of this mission was to obtain a uniform global magnetic field data set of modest resolution, though improved from the earlier POGO mission. With this improved data set, more concise studies of the crustal, external and core components of the earth's geomagnetic field could be undertaken.

The preliminary results from the Magsat mission include a) initial scalar and vector component magnetic anomaly maps (Langel et al.,1982a and Langel et al.,1982b), b) an improved geomagnetic field model, MGST(4/81) (Langel and Estes,1982), c) new information concerning the external field currents e.g., (Maeda et al.,1982), and d) studies of detection and resolution of crustal anomalies. As the present study concerns the crustal component of the Magsat data, only those that research which relates to this topic

will be discussed.

Below I discuss the initial data reduction, analysis and interpretation carried out by those associated directly with the Magsat project. I then discuss my own approach to these problems.

3.2 Magsat Project Data Analysis

One objective of the Magsat mission was to obtain data which would enable improved modeling of magnetic anomalies. The previous set of magnetic satellite data (POGO) was limited to resolution of only large scale features (250-500 kilometers), whereas with the Magsat data the resolution was increased to include features in the range of 150-300 kilometers (Langel et al,1982a). This increase in resolution was accomplished by aquiring data at lower altitudes (200-500 kilometers) as opposed to 400-1510 kilometers for the POGO data set. In areas such as Africa where surface data are hard to obtain, the satellite data should provide a useful data set for geologic modeling.

One major disadvantage to using this type of data is the difficulty in isolating crustal fields from the internal (core) and external magnetic field effects. Other errors are incurred by the satellite position and attitude uncertainty and by instrument effects. Together these increase the uncertainty of the resolution and accuracy of this data.

3.2.1 Data Aquisition

The Magsat spacecraft carried a Cesium vapor scalar magnetometer and a fluxgate vector magnetometer. Attitude determination came from a combination of star cameras, a sun sensor and a pitch gyro. Table 1 lists the estimated errors for each of the two data sets. The data was taken at a rate of 8 samples/second for the scalar magnetometer and 16 samples/second for the vector magnetometer.

The original data set was condensed for easier use. One subset, the "Quiet Days" data set was used to compile the version of the anomaly map for this study, with the area of interest containing over 10,000 data points. This data set includes header data specific to each orbit such as the longitude as the spacecraft passed the equator, and external field estimates for the ascending and descending nodes of the orbit (the satelite was put into roughly a polar orbit; the ascending node starts at the southern end of the orbit and the descending at the northern). For each data point location the satellite geographical position and altitude, estimate of the model core field, and component values are given. The Quiet Days data set is a subset of the Investigator-B data set (one point every five seconds) with a K_p index less than or equal to 2. The K_p indices are a measure of the external magnetic field activity with K_p less than or equal to 2 considered to be magnetically quiet.

3.2.2. Data Reduction

The initial scalar (Langel et al.,1982a) (figure 6) and vector (Langel et al.,1982b) (figure 7) anomaly maps were

derived from the Magsat data by the following steps:

1. selection of data from quiet magnetic periods ($K_p < 2$)

2. removal of a model core field

3. removal of the external field

4. removal of a linear trend

5. elimination of data two standard deviations away from the mean within any two degree block

6. two degree by two degree block averages

Accurate estimates of the core and external field components are important in isolating crustal fields. At Magsat altitudes Langel (1982) estimates the range of magnitudes of the core field from 30,000 to 50,000 gammas, the external field from 0 to 1000 and the remaining crustal contribution from 0 to 50 gammas.

Langel and Estes (1982) computed a new geomagnetic field model (MGST(4/81)) from 15 days of the Magsat data set. They determined that the core field dominates the spectrum for spherical harmonics of degree/order less than fourteen. A spherical harmonic model of degree twelve or thirteen should remove all wavelengths greater than 13.8° ($180^{\circ} / 13$). Langel and Estes' estimates of the model core field are included in the Magsat data set.

After removal of the core field, the external field contribution must be eliminated to isolate the crustal component. This effect is partially removed by using only that data from magnetically quiet periods. The currents giving rise to these time-varying magnetic fields arise

principally in two regions above the earth, the magnetosphere and the ionosphere. The magnetosphere currents flow along magnetic field lines and result from solar wind interaction with the earth's magnetic fields, and the ionosphere currents are confined to a conducting region of the earth's atmosphere. An estimate of the external field is obtained by a similar method to that used for the internal field (it will also be discussed in more detail in a later section). From the form of the external model, coefficients of the external field and internally induced field therefore were computed for each half orbit by a least-squares analysis of the measured field.

The residual remaining after removal of the core and external fields should be the crustal anomaly. Since there still remained orbit-to-orbit biases in the data set (Langel et al.,1982a), a linear trend was fit to segments of each pass (-50° to 0°, -25° to 25°, 0° to 50° latitude). The data were then collected into 2° by 2° blocks and any value greater than 2 standard deviations from the mean of the block was discarded. Averages for each block were then derived. For the scalar anomaly map, an average of 25 points/block existed with an average altitude of 404 kilometers (Langel et al.,1982a). The vertical component vector map averaged 9.4 points/block with an average altitude of 430 kilometers (Langel et al.,1982b).

3.3 Results From Mission

Many of the Magsat papers thus far published have

examined the external field current system. Crustal anomaly studies are limited due to uncertainties in the data resolution and accuracy. Some large scale anomalous features have been correlated with the Magsat anomalies, but the majority of the crustal features are small enough that their magnetic signatures at Magsat altitudes are close to or below the error limits of the data.

Maeda et al. (1982) found evidence for a current system in the equatorial regions. This meridional current system is thought to exist along with the east-west equatorial electrojet, but no direct observations of it have been made. The Magsat orbit was along the dawn-dusk meridian and Maeda et al. (1982), noticed a change in the D-component (eastward) near the duskside dip equator. This change was independent of magnetic activity and appeared on both sides of the dip equator. The amplitude varied from 5 to 25 gammas depending on altitude and geographic location.

Sailor et al. (1982) studied the resolution and repeatibility of the Magsat data. Since the crustal contribution is not time-varying, the data from adjacent orbital tracks should be nearly the same if the crustal contribution dominates the signal. Using coherence analysis, they found the data to be highly coherent along coincident orbits for wavelengths greater than 700 kilometers. Between 700 kilometers and 250 kilometers, the signal-to-noise ratio still implies that significant information exists in the signal despite the low coherence they found in this range.

If 250 kilometers is the lower limit of resolution, then a sample spacing smaller than 1° will contain excessive noise, but one larger could alias this noise unless precautions are taken such as low pass filtering.

In a similar type of analysis, LaBreque and Cande (1984) examined the magnetic anomalies over seamounts in the Central Pacific. They essentially reproduced the results of Sailor et al. (1982), finding that the intermediate wavelength component (1900-700 kilometers) of the data is the most reliable. The decreased resolution of shorter wavelengths (because of satellite instrument and attitude errors) and questionable validity of longer wavelengths due to data reduction techniques limit the data to this range. LaBreque and Cande were also concerned with the added effects of assuming a flat earth approximation for modeling anomalies roughly 400 kilometers in diameter at satellite altitudes. However, in comparing a flat earth upward continued model to a spherical earth model, they found very little deviation between the two.

Galliher (1982) investigated the biases inherent in the crustal component data. He identified the different effects of each type of error (e.g., instrument effects) on the signal. During reduction of the data set for this study, two error effects were encountered. One of these was large variations between two neighboring points (a few gammas difference), which Galliher (1982) relates to error in the attitude determination. The other error type is the inconsistency of data from geographically close orbits,

which is thought to be caused by small scale external effects (Galliher,1982).

The area of interest for this study is confined to Africa, so only the Magsat crustal anomaly studies for this region will be discussed. Regan and Marsh (1982) studied the Bangui anomaly in the stable continental interior of central Africa. This anomaly has one of the highest magnitudes and largest surface area on all of the four published Magsat maps (scalar, X, Y, and Z). Using the total field data, a negative anomaly at the magnetic equater corresponds to a positive susceptibility contrast. The tectonic model Regan and Marsh (1982) devise is uplift during the Precambrian followed by an intrusion of ultramafic material into the crustal rocks with subsequent subsidence and deformation. The magnitude, extent and repeatability of this anomaly enables modeling without the concern of excessive noise effects.

Hastings (1982) looked at correlations between the Magsat scalar map and tectonic map of Africa. He concluded that older Precambrian shield areas have negative anomalies and the younger uplifted areas (e.g. Ahaggar and Tibesti) lower amplitude or positive anomalies. A small low exists between the Ahaggar and Tibesti uplifts and Hastings (1982) describes these features as a crustal block surrounded by basins. The East African rift system has a poor correlation with any scalar anomalies. Hastings (1982) relates this lack to the orientation of the rift system parallal to the

orbital tracks and the delineating effect of magnetic components perpendicular to magnetic north.

Arkani-Hamed and Stangway (1984b) produced their own version of a world Magsat scalar anomaly map (figure 8). Based on this data set and an equivalent layer magnetization method, they converted the magnetic anomalies to lateral variations of magnetization . Assuming that the anomalies are due to lateral variations of the induced magnetization in a magnetized layer, they computed a map of the apparent magnetic susceptiblity variation (figure 9). This map was derived using spherical harmonic coefficients of degree/order 19 to 53 for a magnetized layer 50 kilometers thick covering the entire earth and with a constant susceptibilty in the vertical direction. Another important assumption in this method and subsequent modeling techniques is that magnetic sources can exist below the MOHO. They describe their result as a susceptibility anomaly map in contrast to susceptiblity contrast so that a positive susceptibilty anomaly implies a higher susceptibility of the layer rather than a positive contrast. Using their compiled map, Arkani-Hamed and Strangway (1984a) examined the susceptibility anomalies associated with aulacogens and cratonic regions in Africa and South America. The rise of hot asthenospheric material into the lithosphere should decrease the magnetic susceptibility relative to the surrounding areas and should therefore show a low susceptibility anomaly. By a simple conduction model, they show that as time increases (and the intrusion cools) the

susceptibilty anomaly becomes more positive. Arkani-Hamed
and Strangway (1984a) also calulated the time varying
relationship of depth to the Curie isotherm and total
magnetic susceptibility (figure 10).

3.4 Magsat Data Analysis for North Africa

3.4.1 Data Distribution

As mentioned earlier, the Investigator-B (INV-B) data
set was aquired for this study. This data set was taken over
a 7-month period starting in November of 1979. The 5-second
interval sample rate provided a good coverage along the
orbital tracks.

The global data set, even in computer binary format is
extremely large, so it was necessary to compile a small
subset of the data retaining only those data and header
values needed for the vertical and scalar component
calculations. The compiled subset of the INV-B data
contained only those orbits within the study area that had a
K_p less than 2 creating a data set with approximately
160 orbits and 12,000 data points. Roughly 8% of the total
number of points are bad due to instrument and recording
difficulties. The data was further divided into dawn and
dusk orbits. Figures 11a and 11b show the latitude/longitude
distribution for the dawn (descending) and dusk (ascending)
orbits. The orbits tend to cluster together leaving in some
places $1^{\circ}-2^{\circ}$ gaps. Combining the two data sets
eliminates some of the problem, but the increased external

noise of the dusk (ascending) orbits introduces an additional error. The number of data points/block is lower than the world averages computed by Langel et al. (1982a) and probably results from the orbit spacings being greater at the equater than the poles.

3.4.2 Reduction Techniques

The data was reduced to the respective components and maps derived in a similar sequence as used by Langel et al. (1982a,1982b). As will be discussed later, the Magsat maps from this study do not correlate well with the corresponding published versions. It should be noted that the scalar map produced by Arkani-Hamed and Strangway (1984b) (figure 8) also does not correlate with the published scalar map Langel et al.,1982a). It is not known what reduction methods they employed, but all maps are derived from the same data set. Single orbit profiles were also examined and bandpass filtered following a similar method as used by Sailor et al. (1982).

The first step in the reduction of the data involves removal of the model core and external fields. The external field is derived from the external potential function

$$V = [(r/a)E + (a/r)^2 I] \cos\theta \qquad (1)$$

where (a) is the mean radius of the earth (6371.2 kilometers), (r) the radial distance to the data point, (θ) the dip latitude subtracted from 90° and (E) and (I) the external and induced field coefficients, respectively,

calculated by a least squares procedure. These parameters are all included in the header and data records. Taking the derivative of equation 1 with respect to the (r) and (θ) directions gives the external components

$$DVDR = \cos(\theta) \ [E/a - (2a^2)] \ / \ r^3 I \qquad (2)$$

$$DVDT = -[1/r \ \sin\theta] \ [E(r/a) + (a/r)^2 I] \qquad (3)$$

The model core field for each data point is included with the data set and so the vertical and magnitude anomalies are

$$Z = Z_{data} - Z_{core} - DVDR \qquad (4)$$

$$M = [(H_r - DVDR)^2 + (H_0 - DVDT)^2 + H_o^2]^{1/2} - M_{core} \qquad (5)$$

Trend removal of each orbit was performed using the IMSL routine IFLSQ which uses a least squares apporximation to apply a polynomial fit to the data. A quadratic trend was removed from each orbit and the fit was applied to the 0° to 30^0 range of this data set. Limited computer disk storage space did not allow a larger data range to check the trend removal variations between different size segments.

Elimination of data two standard deviations away from the mean reduced each data set (ascending and descending) approximately 500 points. Enough data existed for 1° by 1° block averages to be computed with every block containing data points. The 1° instead of 2° block size was used because resolution of the magnetic model averaged at 2° was poor. Maps calculated for 1° and 2° averages had very little difference.

The data were gridded and contoured using Radian Corporation's CPS-1 plotting package. A linear projection method was used for gridding and the data were smoothed using a 2-D symmetric operator prior to contouring.

In addition to map presentations, geographically coincident pairs of orbits were selected for filtering and model correlation. The same quadratic trend removal technique was applied to each orbit. It was assumed that the application of a bandpass filter to each orbit should eliminate the need for removal of deviations from the mean and averaging. Prior to filtering, the data along each orbit was interpolated to $1°$ spacing intervals using a Lagrangian algorithm. The bandpass filter operator was tested for ringing at the edges and as a result it was not necessary to apply a taper function.

3.5 Discussion

Arkani-Hamed and Strangway (1984a) and Regan and Marsh (1982) showed that modeling of isolated crustal features close to the 250 kilometer lower limit of resolution can be accomplished (Sailor et al.,1982). These and the other studies mentioned have used the scalar data where the error limits are much smaller than for the component data.

Due to the new evidence for dusk meridional equatorial currents (Maeda et al.,1982), use of only the dawn orbits of the "Quiet Days" data is thought to further reduce the crustal component error in the scalar data. Arkani-Hamed and

Strangway (1984b) used this smaller subset to compile their scalar map. This current system shows a systematic change in the Y-component (eastward) data and would thus effect the scalar data. This current has only a small effect on the Z-component (vertical data).

The deviations between the scalar maps of Langel et al.(1982a) and Arkani-Hamed and Strangway (1984b) leave some doubt as to the validity of correlations between map view anomalies and actual tectonic features. Because of the errors in neglecting altitude variations, data reduction techniques and dawn-dusk subsets, orbit profiles across the hotspots will be compared with profiles across the hotspot models.

The data reduction techniques for this present study are similar to those carried out for derivation of the published maps. As will be later shown, slight deviations from these original methods such as different gridding algorithms as well as analysis over a smaller area create variations between the maps. However, some anomalies are consistent and these are to be the most reliable (e.g. the anomaly associated with the Ahaggar uplift).

CHAPTER 4

HOTSPOT MODELS

4.1 Introduction

Hotspots are defined as intra-plate features caused by a subsurface thermal anomaly. The surface expression of these features is identified by extensive crustal uplifts and in many cases, volcanism. Because of the broadness of this definition, there is much disagreement as to the actual present number of hotspots and, the mantle source and mechanism by which they evolve.

According to Crough (1979), approximately 10 percent of the earth's surface is part of a hotspot swell. This percentage varies among different authors because of the uncertainity in explaining all mid-plate volcanism in terms of hotspots. There is some agreement that ocean depth anomalies (not related to the normal seafloor age-depth relationship) are hotspot features. The correlation on the continents between uplift and volcanism and hotpots is not as certain.

One controversial subject concerning hotspots is their origin. Wilson (1963) first presented the plume theory as a

possible origin for the Hawaiian Islands. This concept was further developed by Morgan (1972) into the hypothesis of fixed mantle plumes. Morgan (1972) describes hotspots as surface manifestations of lower mantle plumes. These plumes bring heat and material up to the asthenosphere and produce horizontal currents which flow radially away from each plume. The return flow is distributed throughout the mantle, which can lead to pressure release melting of the plates and magma penetration. Morgan assumed that these cylindrical shaped plumes have a diameter of approximately 150 kilometers.

4.2 Modeling

It is apparent that the mechanism which produces the high mantle heat flux associated with each swell is not well understood. Along with the increased heat flow, another characteristic of hotspot swells is a small positive Free-air anomaly, implying that the topographic features are isostatically compensated at depth. Crough (1978) looked at a number of swells and calculated root depths (or depth to compensation) within the range of normal lithosphere thicknesses. From these results, he proposed a lithosphere thinning model (as opposed to the emplacement of a mafic body as suggested by other authors). He looked in detail at the Ahaggar (Crough,1981b) and Darfur (Crough,1981a) uplifts in Africa and the relationship between the Free-air gravity and topographic expression of these swells. Considering the

consistency of his results it seems feasible to develop an isostatic model for hotspots. The isostatic model presented in this research is used to define the depth to the Curie isotherm which mimics the compensation depth, but at a shallower level. In some models the velocity of the plate over the hotspot was introduced into the model. Birch's (1975) point source hotspot model was incorporated into the isostatic model, and used to calculate isotherms.

4.2.1 Isostatic Model

Over broad uplifts, the Free-air gravity anomaly is proportional to compensation depth, and so the amplitude of the anomaly can be used to calculate this depth. Based on this relationship and assuming local isostatic equilibrium, Crough (1981b) examined the Free-air gravity anomaly over the Ahaggar uplift. All gravity measurements at elevations above 1200 meters were neglected to eliminate the effects of the high volcanoes and any wavelengths greater than 250 kilometers were eliminated to isolate the gravity signal of the swell. The positive gravity values follow the SW-NE trend of the swell and reach their highest amplitude of 40 mgals near the peak of the swell. Crough (1981b) also assumes a uniform density crust and suggests that any density variations not correlated with topography should appear as random noise in the signal. The hypothetical isostatic model he proposes is shown in figure 4a with (D) being the depth to compensation (or lithosphere/asthenosphere boundary) and (r/2) the amount of

lithosphere thinning that has occurred. The amplitude of the anomaly is best matched to the theoretical model if the root depth is at 60 kilometers. Using a similiar method, Crough (1981a) proposed a root depth between 40 and 80 kilometers for the Darfur swell with a depth of 50 kilometers best explaining the gravity anomaly (figure 4b). In both cases the compensating mass which isostatically supports the swell is in the lower portion of the lithosphere. Crough (1981a) proposes that the lithosphere thinning is due to magma production in the asthenosphere (high heat flux) with rifting, if present, being a secondary process.

The lithospheric thinning mechanism for hotspots is shown schematically in figure 12. The column on the left side shows a normal lithosphere section with thickness (L_R) and asthenospheric heat flux (q_o). The heat flow at the base of the lithosphere increases to (q') inducing a thinning and isostatic uplift. Assuming isostatic equilibrium and ignoring heat sources, the relationship between the two columns is

$$h' \ (\rho_L - \rho_A) = h \ \rho_L \tag{6}$$

The change in temperature or gradient in the normal lithosphere is

$$dT \ / \ dz = (T_a - T_o) \ / \ L_R \tag{7}$$

and under the swell is

$$dT' \ / \ dz = (T_a - T_o) \ / \ L_A \tag{8}$$

where T_a is the temperature at the base of the lithosphere

and T_o is the surface temperature. Since

$$L_A = L_R - (\rho_A / \rho_L - \rho_A) * h \qquad (9)$$

the temperature gradient for the thinned lithosphere can also be expressed as

$$dT'/dz = (T_a - T_o) / [L_R - (\rho_A/\rho_L - \rho_A) * h] \qquad (10)$$

This equation can be used to calculate the depth of compensation beneath the hotspot.

4.2.2 Magnetic Model

Equation 10 can be used to find the depth to the base of the lithosphere. The present study is concerned only with that portion of the lithosphere contributing to the magnetic crustal signal. This region is defined by the Curie isotherm (T_c) (figure 13) and equation 10 can be modified to calculate this depth

$$z_c = (T_c - T_o / T_a - T_o) [L_R - (\rho_L / \rho_L - \rho_A) * h] \qquad (11)$$

The validity of equation 11 for defining the Curie surface depends on what determines the lower magnetic boundary for induction. The susceptibility is affected by temperature, and volume, distribution and mineralogy of the magnetic minerals. According to Haggerty (1978), the mineralogy is the primary factor governing the position of the Curie isotherm. Under low temperature oxidation and stable conditions, the solid solution series Fe_3O_4 - Fe_2TiO_4 determines the Curie points, which range from $580^{\circ}C$ for pure magnetite to $-153^{\circ}C$ for pure ulvospinel.

Wasilewski (1979) studied the magnetic properties of mantle xenoliths and found that the spinels that dominate the mineralogy are non-magnetic at mantle temperatures. He concluded that the MOHO is the lower magnetic boundary. Xenoliths are thought to be good representatives of deep crustal and upper mantle rocks because their rapid accent to the surface preserves their primary mineralogic and magnetic properties. Despite knowing the composition and metamorphic grade for xenoliths, their original position in the crust or mantle, the percentage of material they represent and the amount of contamination during assent is unknown.

According to Wasilewski (1979), the Curie isotherm for pure magnetite would be at approximately 19 kilometers for an average geothermal gradient of $.03^{\circ}C/meter$. In contrast to this Haggerty(1978), studied the distribution of magnetic mineral assemblages and found that magnetic alloys of the Fe-Ni-Co-Cu series have Curie temperatures from $620^{\circ}C-1100^{\circ}C$ and can exist below the MOHO. While the $Fe_2O_3-TiO_2$ oxide series are the most widespread of the magnetic minerals, those alloys resulting from the serpentinization of mafic and ultramafic rocks dominate the magnetic character of deep crustal anomalies. Thus according to Haggerty, it is possible to have magnetic minerals stable at lower crust and upper mantle temperature and pressure conditions.

For the purpose of this research, equation 11 will be used to model the Curie isotherm under the hypothesis of Haggerty (1978) that the Curie isotherm can exist below the

MOHO. The initial modeling of the Curie surface below the hotspots with the simple isostatic model (described in the previous section) did not correlate well with the actual Magsat data. It was necessary to modify the method for defining the Curie isotherm surface to include the effects of plate motion.

4.2.3 Moving Plate Model

Birch (1975) devised a model for hotspots as a point source of heat in an infinite moving half space. A boundary condition for the solution required that the surface temperature go to $0^\circ C$, so to satisfy this he added a negative image source above the upper surface. The equation for the temperature distribution in the slab is

$$T(x,y,z) = (Q/4\pi K) * \left\{ \exp[-(R_1-x)v / 2k]/R_1 - \right. \tag{12}$$
$$\left. \exp[-(R_2-x)v / 2k]/R_2 \right\}$$

where (Q) is the strength of the souce, (K) is the thermal conductivity, (k) is the thermal diffusivity, (R_1) the distance to the source, (R_2) the distance to the image source and (v) the velocity, which is in the X-direction. If the source is located at (x_0,y_0) then

$$R_1 = [(x-x_0)^2+(y-y_0)^2+(ds-z)^2]^{1/2} \tag{13}$$

$$R_2 = [(x-x_0)^2+(y-y_0)^2+(ds-z)^2]^{1/2} \tag{14}$$

with (ds) being the depth of the heat source. For the purpose of modeling, it is necessary to define an arbitrary plate velocity direction that makes an angle (a) with the X-

axis. By defining two unit vectors, (U_r) in the direction from the origin to some point $(x,y,0)$ and (U_v) in the direction (v) (from equation 12) and with

$$R_h = [(x-x_o)^2 + (y-y_o)^2]^{1/2} \qquad (15)$$

the point (x) from equation 12 should be replaced by

$$R_h \; U_R \cdot U_V \qquad (16)$$

The dot product of the two velocity vectors can be expressed as

$$U_R \cdot U_V = \cos(a - \beta) = \cos(\gamma) \qquad (17)$$

if (β') is the angle between (U_R) and a vector from the origin

$$\beta = \tan^{-1}[(y-y_o)(x-x_o)] \qquad (18)$$

The total temperature profile is then

$$T(x,y,z) = T_B(z) + \sum_{m=1}^{n} T_n(x,y,z) \qquad (19)$$

where $(T_B(z))$ is the background gradient expressed as

$$T_B(z) = (dT/dz) \cdot z \qquad (20)$$

and $(T_n(x,y,z))$ is equation 12 for (n) sources or hotspots. An interative forward method can be used to map the depth to the Curie surface using equation 19 to define the temperature distribution in the moving slab and finding at every point the depth at which the temperature is equal to the Curie temperature.

Birch (1975) calculated the depth to the $1300^\circ C$

isotherm or the lithosphere/asthenosphere boundary for a single point source of heat. Figure 14 shows his results for a slab velocity of .01 cm/yr to 10 cm/yr. As the velocity increases, the depth of the isotherm increases and the peak is shifted downstream from the source. The amount of depth variation of this isotherm ranges from 5 kilometers to 45 kilometers at these velocities and surface uplift due to thermal expansion is calculated to range from .1 to .4 kilometers.

CHAPTER 5

METHODS FOR DERIVATION OF A MODEL

5.1 Introduction

In this section, the methods utilized for the model derivation are discussed. The final results as well as correlations between the magnetic model and reduced data will be presented in the next section. The methods employed for this study are twofold. First, it was necessay to devise a way to model the magnetic signature of the hotspots and second to reduce the Magsat data for correlation with the proposed model.

Parker (1972) developed a Fourier transform technique for calculating potential fields due to an uneven layer of material. This method provided a convenient way to model the three hotspots. Gridded surface topography was used as the upper boundary of the layer. A lower boundary was needed to incorporate the subsurface effects of the hotspots. In the previous section, the methods used to calculate the lower surface (or Curie isotherm surface) were discussed. The size of the area of interest was large enough that the assumption of a flat earth approximation

needed to be checked. The Fourier transform algorithm could be modified for a spherical surface, but for computational purposes this extension would be difficult.

It was necessary to modify the original algorithm for variable magnetization direction and so a geomagnetic field model for north Africa was generated.

5.2 Magnetic Model

5.2.1 Geomagnetic Field Calculations

The time and spatial varying nature of the earth's internal magnetic field requires the derivation of a geomagnetic field model corresponding to the location and time of data aquisition for the proposed magnetic model. The first such representation was done by Gauss in 1839 using a series of spherical harmonic coefficients of the internal potential. Limited by data distribution, Gauss calculated a model of degree 4. Present day geomagnetic field models used to isolate crustal and external fields from internal (core fields) are extended to around degree/order 23. The cut-off between the core and crustal source contributions can be computed using the power spectrum of the spherical harmonic coefficients.

According to Gauss, the potential of the internal geomagnetic field can be represented by

$$V = a \sum_{n=1}^{N} \sum_{m=0}^{n} (a/r)^{n+1} [g_n^m \cos m\phi + h_n^m \sin m\phi] P_n^m (\cos\theta) \quad (21)$$

where (r), (θ) and (ϕ) are the standard spherical coordinates, (a) the mean radius of the earth, (P_n^m) the

Schmidt quasi-normalized form of associated Legendre functions and (g_n^m) and (h_n^m) are the spherical harmonic coefficients. The components of the earth's field are then

$$X = (1/r)(dV/d\theta) \tag{22}$$

$$Y = (-1/r \sin)(dV/d\phi) \tag{23}$$

$$Z = (dV/dr) \tag{24}$$

with (θ) being the geocentric colatitude. With equations 22, 23 and 24 any element of the earth's magnetic field can be computed using the following trigometric relationships

$$D = \arctan (y/x) \tag{25}$$

$$I = \arctan (y/H) \tag{26}$$

$$F^2 = H^2+Z^2 = X^2+Y^2+Z^2 \tag{27}$$

where (D) is the declination, (I) the inclination, (H) the horizontal intensity and (F) the total intensity.

A FORTRAN program was written to calculate the components of the geomagnetic field at any specified latitude and longitude. The derivation of the proposed model needed the inclination and declination at each model data point location. The inclination of the earth's field for the study area in north Africa varies from -1° to $+40^\circ$ with the lines of constant inclination roughly parallel to the lines of latitude. The declination is approximately -6° in the southwest corner of the study area and increases in a northeasterly direction to $+3^\circ$.

The spherical harmonic coefficients (gm and hm) used in the calculation of the field model were the MGST(6/80) model

data. Calculated by Goddard Space Flight Center, these were the first set derived from the Magsat data for the main field at epoch 1979.5 and contain coefficients up to degree/order 13.

The spherical harmonic degree/order terms used for the International Geomagnetic Reference Field published by the Department of the Interior are up to and including m=n=10. Langel and Estes (1982), in calculating the power spectrum of the Magsat spherical harmonic coefficients up to degree/order 23 found a distinct change in slope at degree/order 14 and believe this cutoff is the term at which the main field becomes dominated by the crustal component. This study is relatively recent and until further work is done, the IGRF model convention will be used as a standard.

5.2.2 Flat Earth Approximation

The method for defining the magnetic model assumes the magnetized layer is flat (i.e., neglects curvature of the Earth). The FFT algorithm for calculating potential anomalies within a flat layer had previously been applied to areas with dimensions of a few degrees. Due to the size of the study area (20° by 30°) and the altitude of the satellite, it was necessay to determine the error induced on the model results by assuming a flat earth. LaBrecque and Cande (1984), studying the magnetic anomalies of central Pacific seamounts over an area of 20° by 50° also examined the flat earth approximation.

The calculation used to compare the error between a flat and spherical surface at some altitude above the surface consisted of looking at a very simple sphere model. The sphere was divided into circular shells concentric around the top (e.g. North Pole). The susceptibility of the shells alternated positive to negative and the thickness remained constant. The vertical magnetic component was calculated at a particular height for each shell with the angle from the vertical to each shell increasing from 0° to 180°. This similiar method was applied to the circular shells lying on a flat plane and the percentage difference between the two at each angle was calculated. It was found that for wavelengths between 300 and 700 kilometers and angles up to 45°, the error induced by assuming a flat earth was less than 4 percent at an altitude of 410 kilometers. This error percent is somewhat less than the uncertainty inherent in the Magsat data and because of the complexity involved in modifying the modeling procedure for a spherical surface, the flat earth approximation was adopted.

LaBrecque and Cande (1984) examined the deviation between an upward continued spherical earth and flat earth model of two prisms at 100 kilometers depth within their study area. The error of the flat earth model was less than 10 percent. For simplicity in modeling and computation, they also assumed a flat earth.

5.2.3 Parker Fourier Transform Algorithm

The technique used to model the hotspots developed by

Parker (1972) consists of using a series of Fourier transforms of the magnetic potential to calculate the magnetic anomaly due to an uneven layer of material. The original method assumed a layer with a uniform distribution of magnetization, which is applicable only to small areas (e.g. a few degrees). It was necessary to modify this procedure to allow for variable direction of magnetization. The upper boundary of the layer is the actual topography of the study area and the lower boundary is the calculated Curie isotherm surface.

Parker's (1972) derivation provides a computationally fast method for determining the magnetic and gravitational potential and because the observation plane lies above the layer of material, it is a useful technique for modeling at satellite altitudes. Parker starts with the Fourier transform of the potential equation and manipulates it until it is a sum of Fourier transforms. The anomalous field is then produced by using the inverse transform. In the numerical example Parker presented, he found the series of Fourier transforms to converge well as long as the observation plane does not fall below the upper surface.

The derivation starts with the equation for the magnetic potential of a body of material with a constant direction of magnetization

$$A(r_o) = -\int_V M(\underline{r}) \cdot \nabla(1/|r_o - r|) dv \qquad (28)$$

but with variable intensity such that

$$M(\underline{r}) = \underline{M}_o M(\underline{r}) \qquad (29)$$

where (M_o) is the unit vector in the direction of magnetization. Since

$$M(r)\cdot\nabla = |M|\ d/d\alpha\ =\ M(r)\ (d/d\alpha) \qquad (30)$$

with (α) being the direction of magnetization, equation 28 can be rewritten in terms of two surfaces $(g(r))$ and $(h(r))$ as

$$A(r_o)\ =\ -d/d\alpha \int_0^h M(r)ds \int_g^h dz/|r_o - r| \qquad (31)$$

Defining a new term $(A'(r_o))$ such that

$$A(r_o)\ =\ d/d\alpha A'(r_o)\ =\ M_o\cdot\nabla(A'(r_o)) \qquad (32)$$

and so

$$A'(r)\ =\ -\int_0 M(r)ds \int_g^h dz/|r_o - r| \qquad (33)$$

Taking the Fourier transform of both sides

$$F[A'(r_o)]\ =\int_\chi ds_o\int_0 M(r)ds\ \exp(i|k|r_o)\ \int_g^h dz/|r_o-r| \qquad (34)$$

Equation 34 is then Parker's (1972) notation defined for two uneven surfaces. Changing the order of integration, carrying out the last integral and performing the (z) integration (Parker,1972), equation 34 becomes

$$F[A'(r_o)]\ =-\exp(-|k|z_o)\sum_{n=1}^{\infty}|k|^{n-2}/n!$$
$$F\ [M(r)(h^n(r)-g^n(r))] \qquad (35)$$

The term $(A'(r_o))$ can also be defined in relation to a plane $(A(k_x,k_y))$ denoted by a vector (r_o) at a height (z_o) above the reference surface such that

$$A'(r_o) = -1/(2\pi)^2 \int_{-\infty}^{\infty} \int_{-\infty}^{\infty} \exp(-|k| z_o) A'(k_x, k_y) \qquad (36)$$
$$\exp(ik_x x_o - ik_y y_o) dk_x dk_y$$

where

$$A'(k_x, k_y) = \sum_{n=1}^{\infty} |k|^{n-2}/n! \; F[M(r)(h^n(r) - g^n(r))] \quad (37)$$

and since

$$\nabla A'(r_o) = (d/dx_o \; i + d/dy_o \; j + d/dz_o \; k) A'(r_o) \quad (38)$$

The Fourier transform of this becomes

$$F[\nabla A'(r_o)] = -(ik, |k|) \; F[A'(r_o)] \qquad (39)$$

Following the relationship between $(A(r_o))$ and $(A'(r_o))$ (equation 34), the transform of $(A(r_o))$ is

$$F[A(r_o)] = -\underset{\sim}{M}_o \cdot (ik, |k|) \; F[A'(r_o)] \qquad (40)$$

The components of the magnetic anomaly can be derived using the relationship

$$H = - \nabla A \qquad (41)$$

with the transforms being

$$F[H_x] = ik_x \; F[A(r_o)] \qquad (42)$$

$$F[H_y] = ik_y \; F[A(r_o)] \qquad (43)$$

$$F[H_z] = |k| \; F[A(r_o)] \qquad (44)$$

Parker's method can be modified for variable direction of magnetization with

$$F[A_i(r_o)] = -\exp(-|k| z_o) \sum_{n=1}^{\infty} |k|^{n-2}/n!$$

$$F[M_i(r)(h(r) - g(r)] \quad (45)$$

and

$$F[A(r_o)] = - \left[-ik_x F[A'_x(r_o)] + \right.$$ (46)

$$\left. ik_y F[A'_y(r_o)] + |k| F[A'_z(r_o)] \right]$$

along with equations 42, 43, 44, the magnitude or vector components of the magnetic anomaly due to the layer of material can be derived.

Gridded topography was used as the upper surface of the layer. The lower surface was originally calculated using equation 11 as a function of topography, temperature and density. This equation is very sensitive to variations in density, even within the plausible ranges for crustal, lithospheric and asthenospheric densities, the Curie isotherm varied from depths of 0 to 80 kilometers, and so Crough's (1981a,1981b) results were used to constain the range used. This method presented a problem in that the Curie isotherm was at its shallowest point directly under the volcanoes and it essentially mimics the surface topography. As shown by Birch (1975), for a moving plate the highest temperature gradient lies downstream from the source where the topographic expression is subsiding due to cooling. Incorporating Birch's (1975) derivation, the lower surface was then defined as a function of plate velocity and angle, source strength, depth and position and Curie temperature. With both derivations, a reference lithosphere (unpertubated) thickness is needed. As will be discussed in the next section, significant changes in Curie isotherm

depth require extremely large variations in the parameters.

A FORTRAN program was coded to calculate the vertical and scalar magnetic anomalies. Prior to transforming the upper and lower surfaces, they were combined with the direction cosines of the main field. These cosines are in the (x), (y), and (z) directions and can be calculated from sines and cosines of the inclination and declination. The surfaces were transformed using an IMSL Fast Fourier Transform routine (FFT3D) which calculates the transform of a complex valued 1, 2 or 3 dimensional array. In the transform domain the (X), (Y) and (Z) components are defined and by performing the inverse transform, the desired magnetic anomaly is recovered.

The parameters necessary for the anomaly calculation include the plate velocity and direction, source strength, position and depth for each hotspot source, Curie temperature, average altitude, susceptibility and average field strength for the entire area and reference lithosphere thickness. The numerical values used as well as the modeling results will be presented and discussed in the next section.

CHAPTER 6

RESULTS

6.1 Data/Model Correlation

Through examination of the vertical and scalar component and the ascending and descending data sets of each, a better understanding of the limitations of this type of data were gained. The final fixed and moving plate models are those that best fit the two magnetic field component maps in terms of both anomaly positioning and magnitude. Reasonable variations in the parameters did not alter the two models a great deal, so the models to be presented are felt to be a good simple representation of the three hotspots.

Using Birch's (1975) method for calculating the temperature due to a point source of heat beneath an infinite slab, the fixed (velocity = 0) and moving plate model field signals were calculated. It was assumed that the present day thermal anomalies lie directly below the most recent volcanics of Ahaggar, Tibesti and Darfur. Following Crough's (1982b) results for the lithosphere/asthenosphere boundary (1200° C isotherm) being at approximately 60

kilometers beneath Ahaggar, the Curie isotherm (550° isotherm) lies at roughly 25 kilometers. Using this depth as a starting point, the depth and strength of source and plate velocity and direction were varied to fit the magnetic data. If one assumes that the African plate is moving, the plate velocity for North Africa lies between .5 and 1 cm/yr in a northeasterly direction (Duncan,1982). The best fit with the Magsat anomalies required a moving plate model velocity of .75 cm/yr and azimuth of 35° in a northeasterly direction.

The parameter differences between the fixed and moving plate models are reflected in the source strength and depth. For a fixed plate, the heat loss is concentrated in a smaller area, so it was necessary to decrease the source strengths somewhat to reach the same temperature of the moving plate. As will be seen with the Magsat maps, the Tibesti and Darfur model anomalies are not consistent in position or magnitude with any data anomalies, which was another factor in the choosing the source parameters. The parameters used for the two models are shown in table 2.

Figures 15a and 15b show the depth to the Curie isotherm for the moving and fixed plates, respectively. As is to be expected, the shallowest point on the moving plate surface is shifted downstream from that of the fixed plate which lies directly below the highest portion of the topography (figure 2).

Calculation using the previously discussed modification

to Parker's (1972) technique for the magnetic signatures due
to a layer of material defined by the topography as the
upper boundary and the fixed and moving plate Curie surfaces
as the lower boundary required estimation of four more
parameters. An average altitude for the satellite over the
study area was calculated to be 410 kilomters. The ambient
magnetic field at this altitude was determined to be 40,000.
The one parameter that was difficult to estimate
was the susceptibility contrast. Variations in this contrast
are directly proportional to changes in the magnitude of the
anomaly. By definition, below the Curie isotherm the
susceptibility is 0, so it was a matter of estimating a
susceptibility for the magnetized layer. Assuming a constant
susceptiblity for the entire area is obviously a strong
limitation in this model. The lower surface does fall below
average crustal thicknesses (roughly 35 kilometers) adding
another factor to be considered. For silicic material the
susceptibility averages around 400 ($x10^6$ emu) and for mafic
averages 13,000. Considering all of these factors as well as
matching the anomaly magnitudes, a susceptibility contrast
of 6500 was used.

The vertical component magnetic anomalies due to the
moving and fixed plate models are shown in figures 16a and
16b respectively. The Ahaggar anomaly is well defined in
both models. The center of the anomaly for the moving plate
model is shifted roughly 5° in the direction of plate
motion. The anomaly for Tibesti, though not as well defined,
shows the same shift. As to be expected, a slight positive

anomaly lies to the north of the respective lows. Any effect due to the Darfur hotspot has been washed out by the other two anomalies.

The scalar component models, shown in figures 17a and 17b (for the moving and fixed plate models) do not have as pronounced anomalies as for the vertical component. A similiar shift of roughly 4° in the peaks of the anomalies occurs as does the absence of the Darfur anomaly.

Comparison of these magnetic models with the respective versions of the published maps, shows a fairly good correlation for the moving plate models. The position of the modeled vertical anomaly associated with Ahaggar fits well with the Magsat data anomaly (figure 7). Both show the same northeasterly trend. The Tibesti anomaly has a magnitude below the error limits of the data. The Magsat scalar map (figure 6) does not have the distinct closed anomalies, but a portion of the Meditranean positive in the north extends south over Ahaggar and its positioning correlates with the moving plate model. In both published maps, the Bangui anomaly appears to obliterate any other smaller features in that area.

With any correlation between the Magsat data set and a model, the error limits of the data must be considered. The vertical component data contain the uncertainty in spacecraft attitude, but should be effected very little by the meridonial currents. The attitude error does not effect the scalar data, but the external currents do.

Figures 18a, 18b and 18c display the calculated 1° averaged vertical component, ascending (dusk) data only and descending (dawn) data only maps, respectively. The map for the total data set is extremely noisey and has no correlation with the published version. The ascending orbit map shows the pronounced low associated with Ahaggar also apparent on the decending orbit map although not as distinct. The fixed plate model does not correlate with any of the vertical component maps, but the Ahaggar anomaly fits fairly well with that on the ascending orbit map. It is however hard to justify use of only the ascending orbit data and also how the spacecraft attitude error effected the data.

For the scalar data, the dusk equatorial currents should introduce a noise effect into the ascending (dusk) orbits. This effect appears to be very pronounced as the calculated scalar map (figure 19a) is very similar to the ascending orbit map (figure 19b). The descending orbit map (figure 19c) correlates with the published scalar map. The similar dip in the positive anomaly in the northern portion of the map occurs as does a slight low to the south The positve model anomaly associated with Ahaggar for the fixed plate model is shifted west from the anomaly of the Magsat data.

The correlation between the Magsat and model anomaly for Ahaggar prompted a further look into profiles across each. This anomaly is the only one with any consistency and magnitude above the error limits of the data. Figure 20

displays the initial correlation between corresponding profiles across the Ahaggar anomaly models and the published vertical component map. The moving model appears to fit quite well, but as has been shown this correlation is severly limited by the noise inherent in the data.

6.2 Data Profiles

Pairs of geographically coincident orbits were selected from the ascending and descending data sets that crossed over the Ahaggar anomaly. The same bandpass filter was applied to all the orbits with cutoffs of 700 and 2000 kilometers. The cutoffs were selected as a result of the work done by Sailor et al. (1982) on orbit-to-orbit data reliability. Figures 21-26 display the results of the orbit examination containing the latitude/longitude position, the data with the quadratic trend removed and comparison after filtering of the two corresponding orbits.

Due to the equatorial external currents, the ascending (dusk) orbits for the scalar should be noisier than the descending (dawn). Figure 21 is the dawn orbit and figure 22 the dusk. This added noise is not apparent, but for the filtered versions of these orbits (figures 23a and 23b) the consistency orbit-to-orbit is better for the dawn data. The altitude difference between the coincident orbits is greatest for #326-#2606 being 165 kilometers and 75 kilometers for #2630-#1322.

The vertical data contains considerable noise as

seen in figure 24 (dawn orbits) and figure 25 (dusk orbits).
Orbits 326 and 2606 appear to be phase shifted (figure 26a).
A similar occurrence was found in the other dawn orbits not
presented. The dusk orbits showed a better correlation
(figure 26b).

It was hoped that by examining single orbits, a
clearer understanding of the reliablity of the different
data sets would be obtained. What was gained by this profile
examination was first that the altitude variation between
different orbits had only minor attenuation effects. It was
apparent that the descending (dawn) scalar data showed
better consistency orbit-to-orbit than the dusk data, and
probably a result of the nature of the meridional current
system. The vertical data (both dawn and dusk orbits) show a
distinct phase shift orbit-to-orbit. It is possible that
this is the effect of attitude error on the data set. It is
apparent from examining single orbit profiles, that the
calculation of a contoured map is necessary to help filter
out these errors inherent in the magnetic satellite data.

CHAPTER 7

CONCLUSIONS

The conclusions of this study are constrained by the quality of the Magsat data and simple nature of the model. Originally, it was planned to examine and model the three volcanic regions in north Africa, but as has been shown the magnetic anomaly associated with Ahaggar is the only one which consistently appears in the different data sets. An explanation for this limited correlation is that the topographic swell of Ahaggar covers over twice the surface area of the other two producing an anomaly above the noise error of the data. It is also interesting to note that this volcanic region is not presently geothermally active.

Examination of the orbit data clearly showed the limitations of this data set. The vertical component data set was extremely noisey probably resulting from spacecraft attitude variations. The phase shifts between orbit profiles in this data set were not expected and are probably due to the attitude error. The effects of the equatorial currents in the Y component and subsequently the scalar anomaly decreased the orbit-to-orbit consistency. It appears that

the block averaged maps are more reliable with some of the noise being filtered out by averaging.

Consistency between the different versions of the maps is not what was hoped for. The published scalar map and the descending vector magnitude do show the same positive anomaly trend around the Ahaggar region. A similar correlation for this area exists between the vertical map (Langel et al.,1982a) and ascending data maps. The calculated maps do not fit well with their corresponding published map versions despite similar reduction and computational methods.

The proposed hotspot model is consistent with other techniques applied to thermal anomalies in the lithosphere. Bermingham et al. (1983), calculating a gravity model for the Darfur dome, determined that the lithosphere is roughly 60 kilometers thick beneath the dome. Their model assumes a density contrast of the anomalous material of .05 g/cm3. Using POGO satellite data over the rift valleys in Africa, Jain and Regan (1982) calculated that the Curie isotherm must lie at a depth of 19 kilometers. Both of these models as well as the ones presented are consistent with Crough's (1981a,1981b) isostatic models. The major limitation of the method used for this study is the assumuption of laterally constant parameters within the layer. With little being known about the crustal thickness and lithology in this area, this model is permissible.

Despite the data limitations, the results of this study

favor a moving plate model. Evidence for this conclusion from previous work and the present study can be summarized as the following:

1. the results of Duncan (1981), Chase (1978) and McKenzie and Sclater (1971) all indicate a northeast rotation .5 - 2 cm/yr for the African plate.

2. present day stress directions for Ahaggar are perpendicular to the northeast rotational direction (Yee-han Ng, 1983).

3. positioning of Arkani-Hamed and Strangway's (1984a) susceptibility anomalies lie in a northeasterly direction from present day domes, presumably resulting from the Curie isotherm reaching its shallowest depth roughly 40 Ma after the initial implacement of the thermal source.

4. correlation of published vertical map anomalies with those of the moving plate model anomalies.

5. fixed plate model anomalies lie west of the corresponding ones on the Magsat maps (figure 27a).

6. moving plate model fits well with the scalar component anomalies (figure 27b).

7. correlation between the anomaly associated with the Ahaggar region and those on the ascending vertical data and descending scalar data maps.

Further work needs to be pursued in eliminating the

noise in the data to isolate the true crustal magnetic signal before more conclusive modeling of anomalous features can be accomplished.
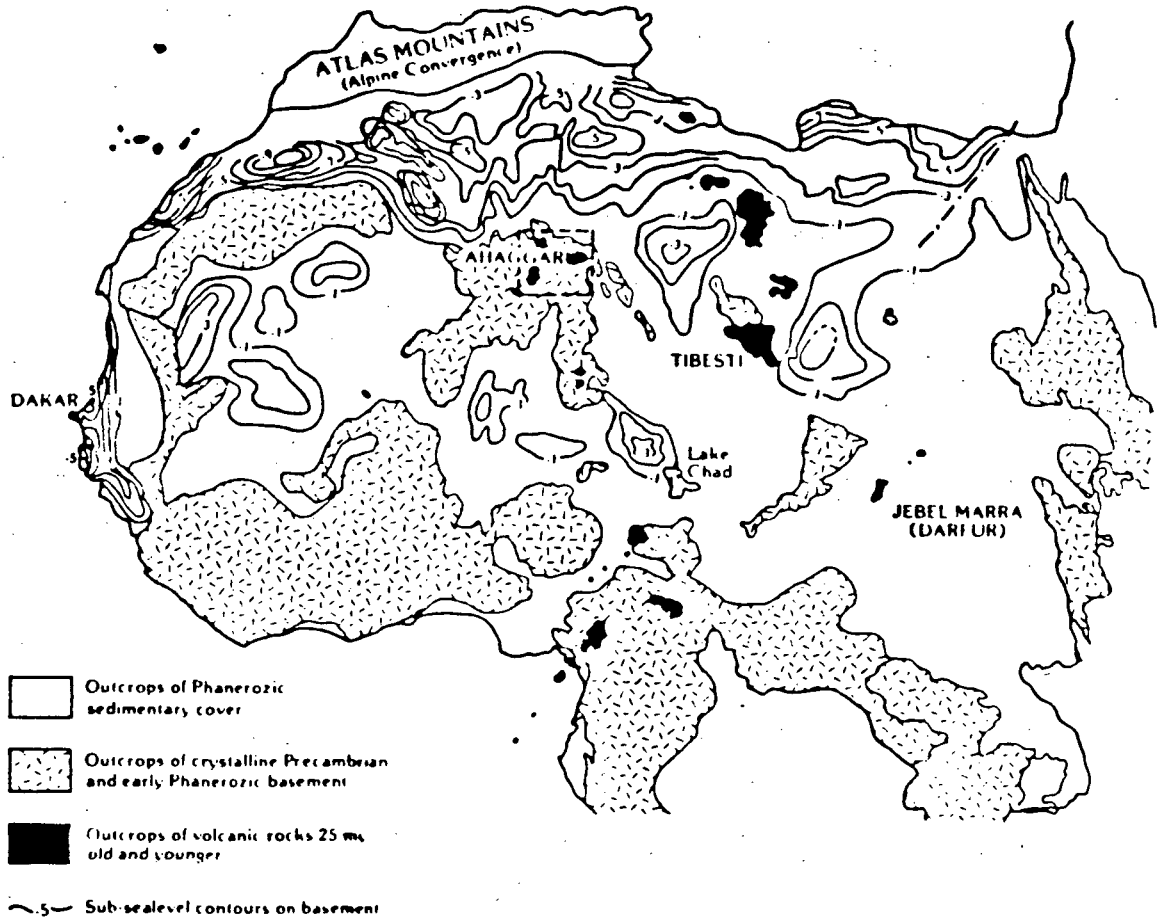
FIGURE 1. Map showing the distribution of basement rock outcrops in North Africa and contours on the depth to basement in areas where it is buried under Phanerozoic cover. Black areas represent volcanic rocks, of proposed hotspot origin, erupted over the last 25 m.y. (based on the Tectonic Map of Africa, UNESCO, 1:5m, 1971).

TOPOGRAPHY
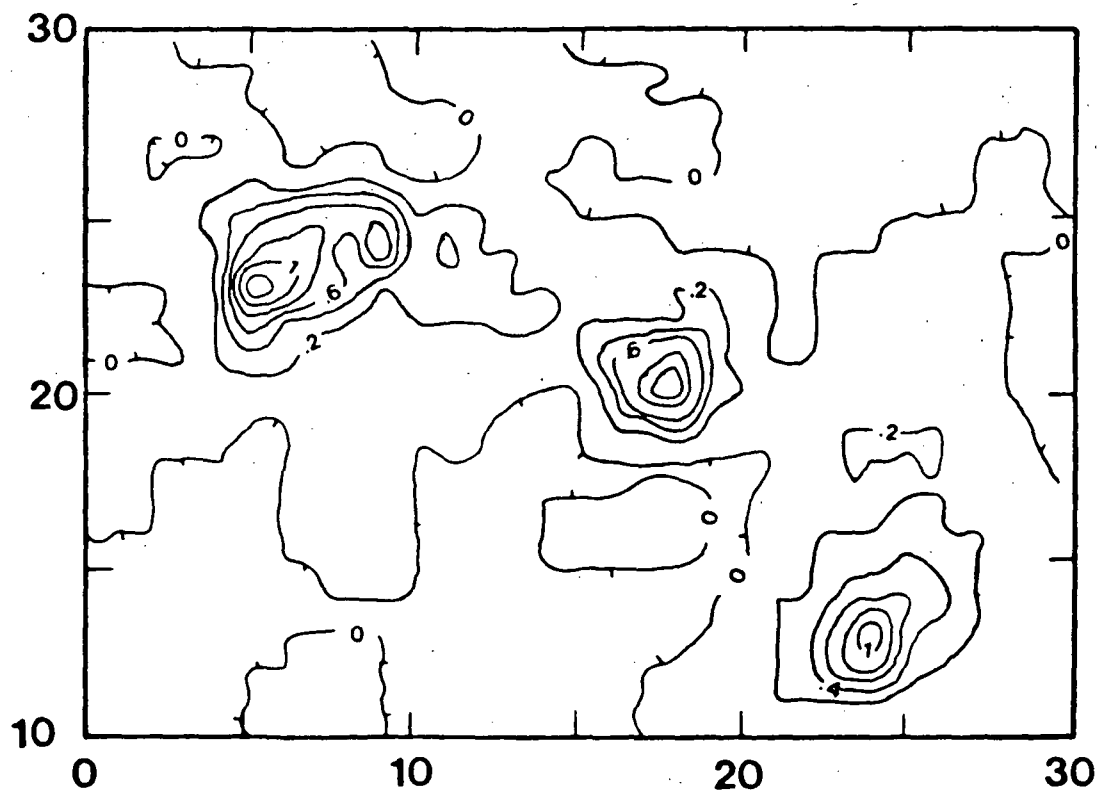
FIGURE 2. Contour map of gridded quarter degree topography data. Contour interval is 200 meters.
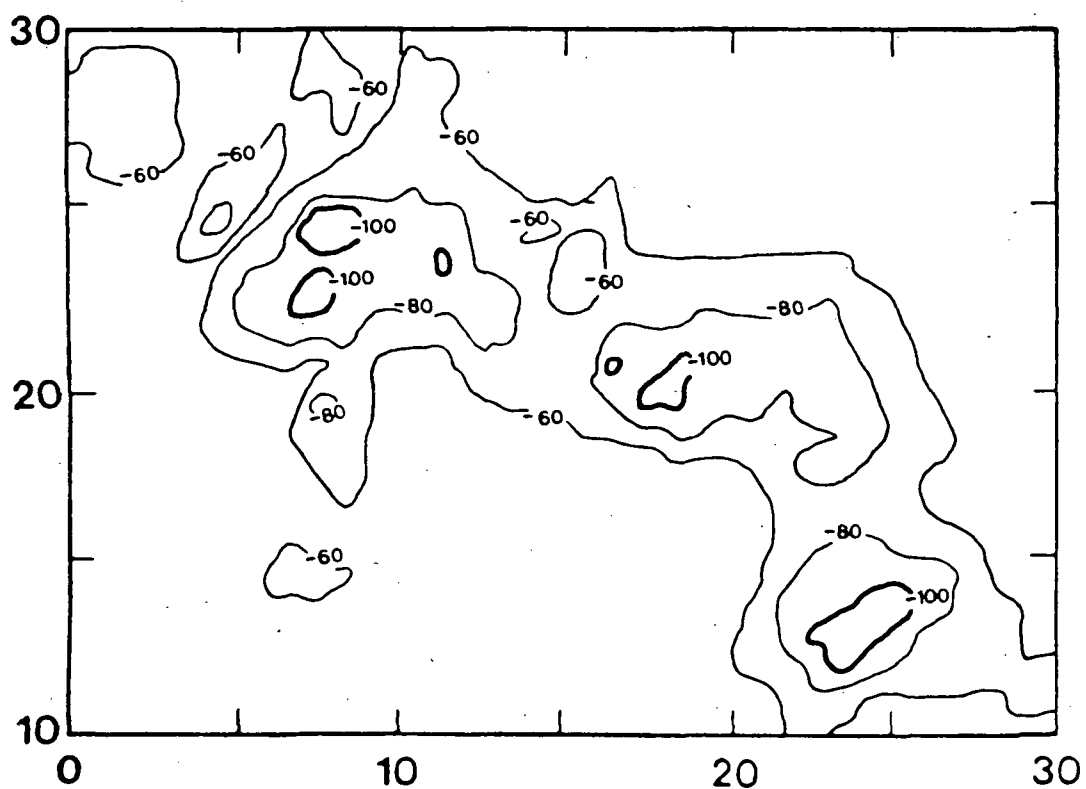
FIGURE 3. Bouguer gravity anomaly map illustrating the continuous feature connecting the Adrar (1), Ahaggar (2), Tibesti (3) and Darfur (4) volcanic provinces (after Bermingham et al., 1983).

ISOSTATIC COMPENSATION MODEL

a
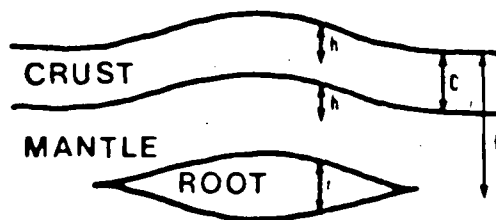
DARFUR GRAVITY MODELS

b
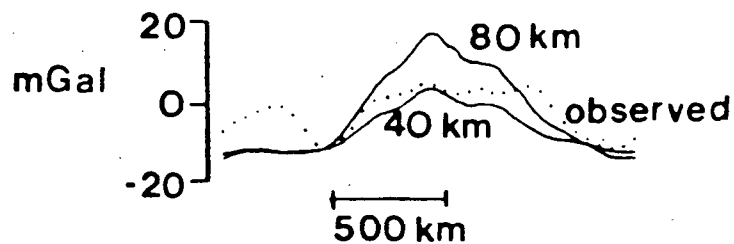
FIGURE 4. Isostatic compensation model showing in (a) the low density root in the mantle which causes the surface uplift and (b) the model applied to the observed free-air gravity across Darfur for root depths of 40 and 80 kilometers (after Crough, 1981a, 1981b).

AFRICAN HOTSPOTS
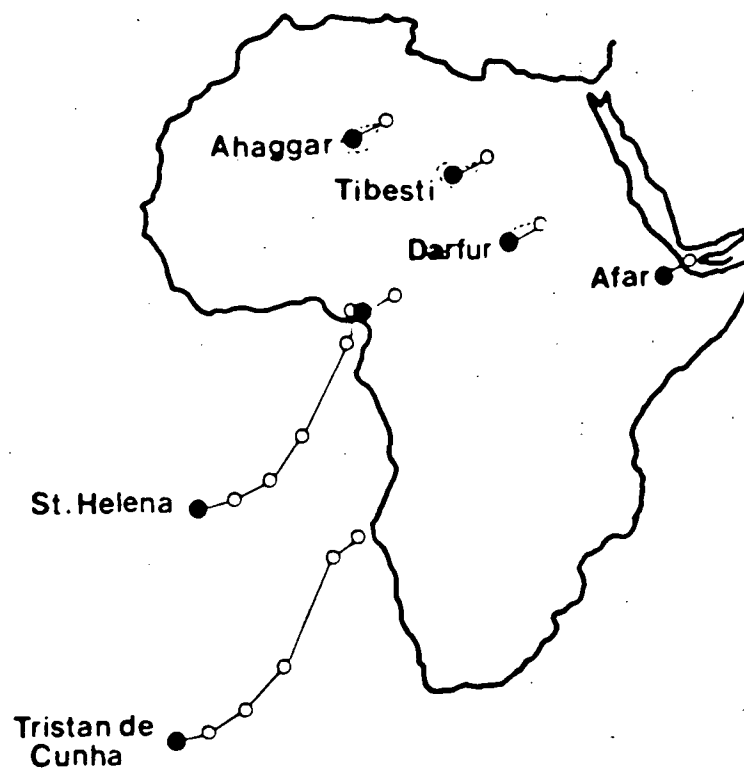
FIGURE 5. African hotspot motion since 100 ma. Presently active hotspots are large filled circles of 1 degree diameter connected by bubbles of 20 my age increments (after Duncan, 1981).

FIGURE 6.

Published Magsat scalar anomaly map (after Langel et al., 1982a).

MAGSAT SCALAR ANOMALY MAP
RELATIVE TO MGST (4/81) MODEL
AVERAGE ALTITUDE: 404 km AVERAGE PTS. 2° x 2° BLOCK × 25

NOVEMBER 1981
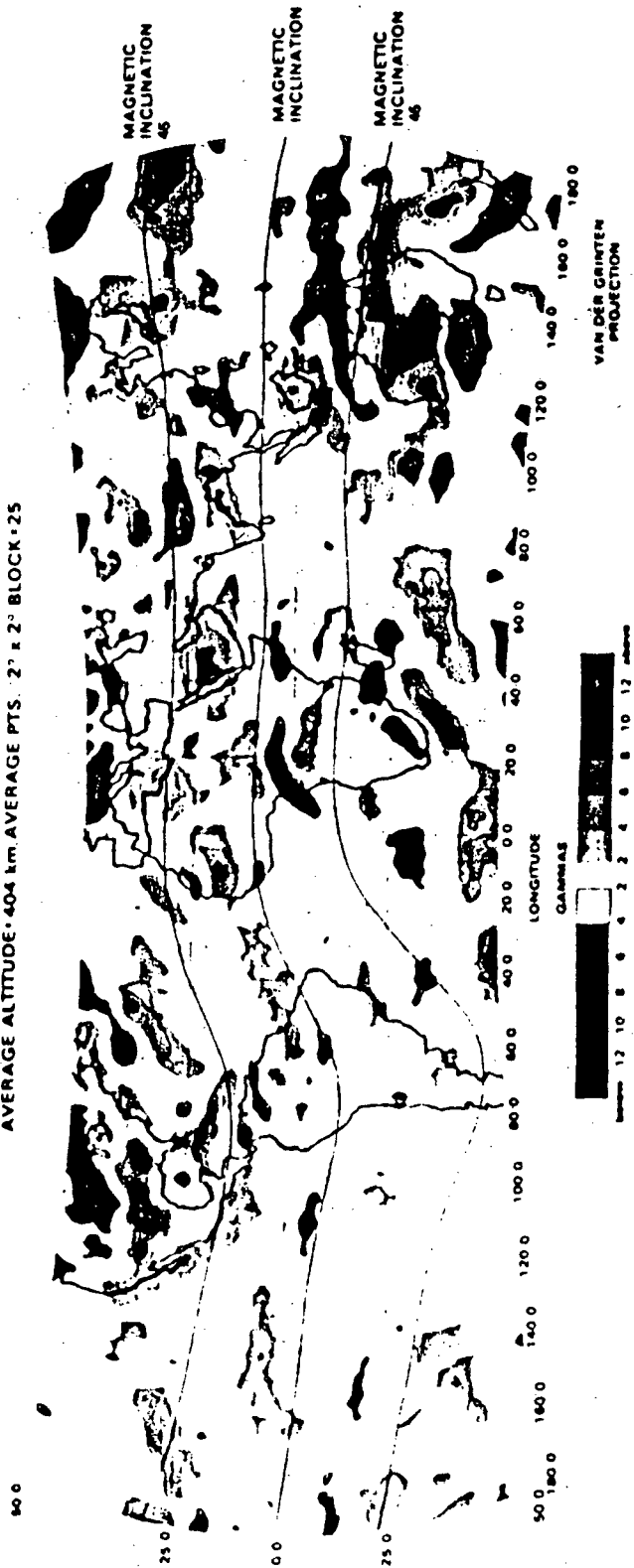
VAN DER GRINTEN PROJECTION

FIGURE 7

Published Magsat vertical anomaly map (after Langel et al., 1982b).

MAGSAT ANOMALY MAP

DELTA Z CONTOURS
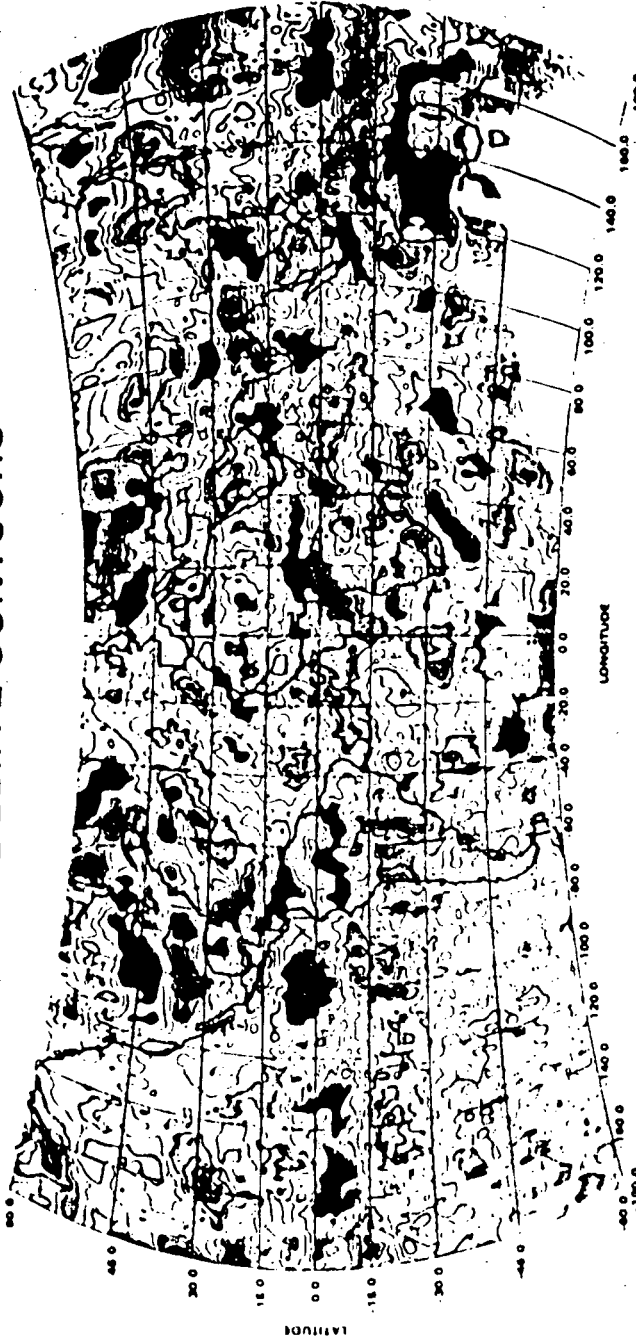
FIGURE 8.

Scalar magnetic anomaly map (after Arkani-Hamed and Strangway, 1984b).
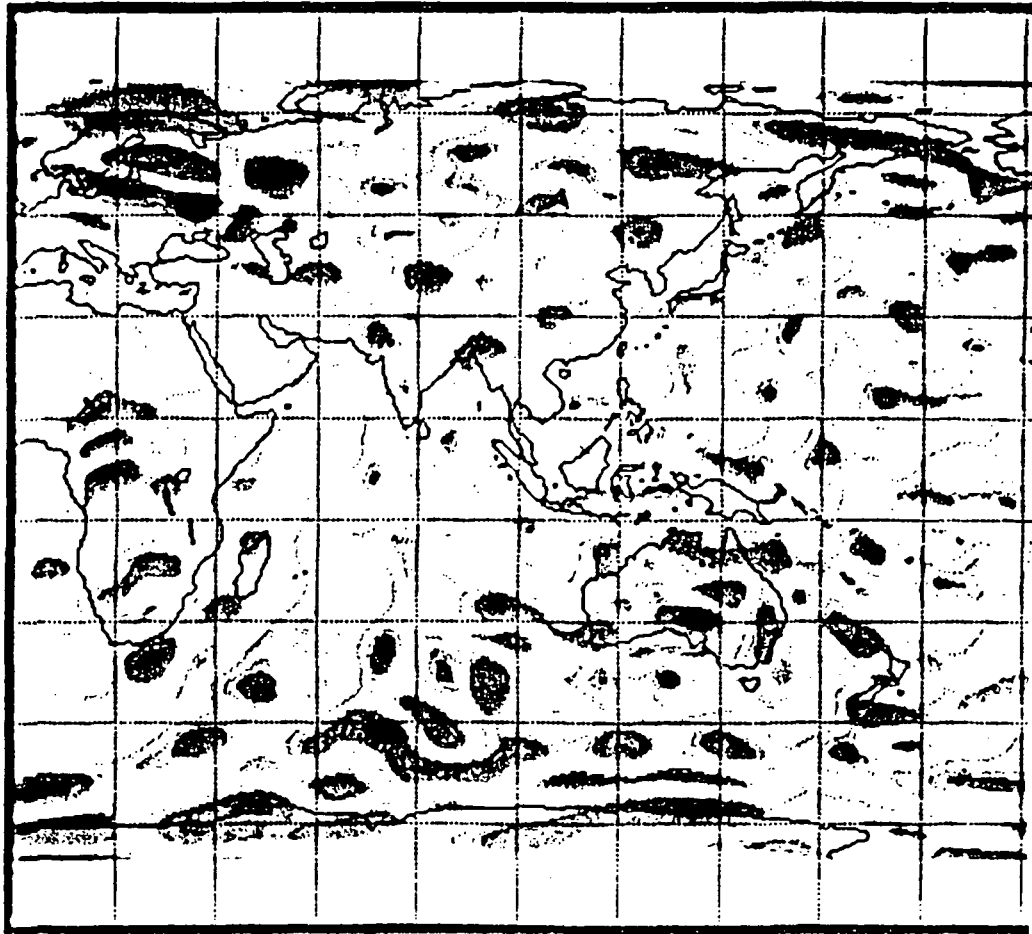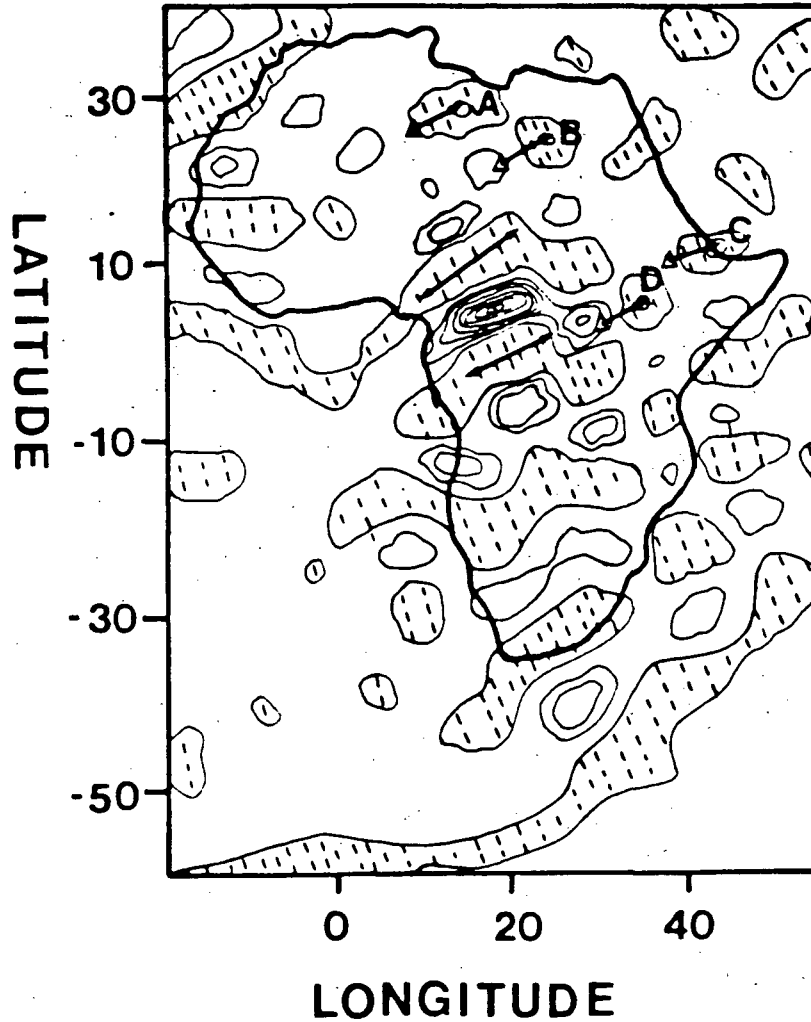
FIGURE 9. Magnetic susceptibilty anomalies. Shaded regions show positive anomalies and triangles the present day position of Ahaggar (A), Tibesti (B), the Ethiopian swell (C) and the East African swell (D) (after Arkani-Hamed and Strangway, 1984b).
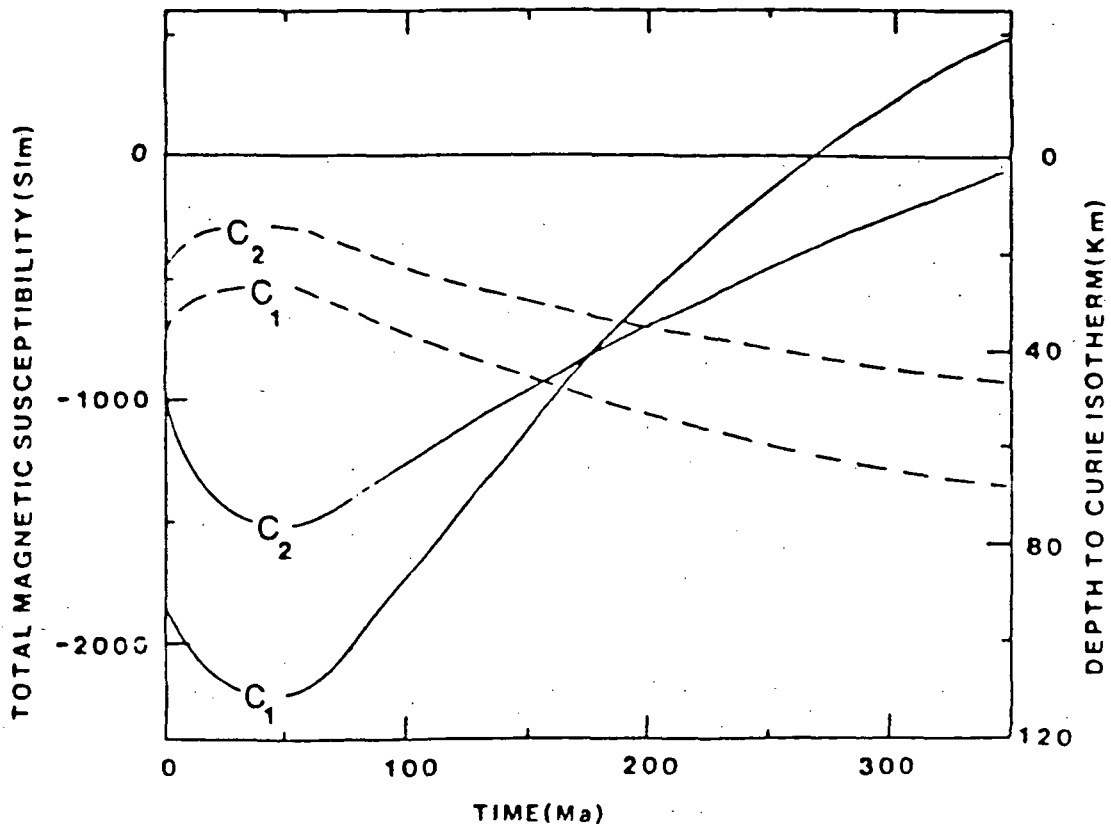
FIGURE 10. The time variations of the total magnetic susceptibility anomaly of the lithosphere (solid lines) and depth to the Curie isotherm (dashed lines) with C1 the cold and C2 the hot continental lithospheres (after Arkani-Hamed, 1984a).
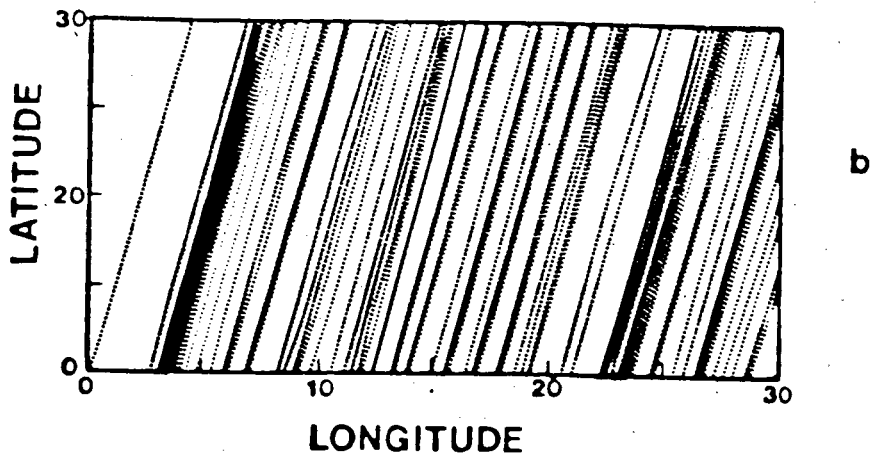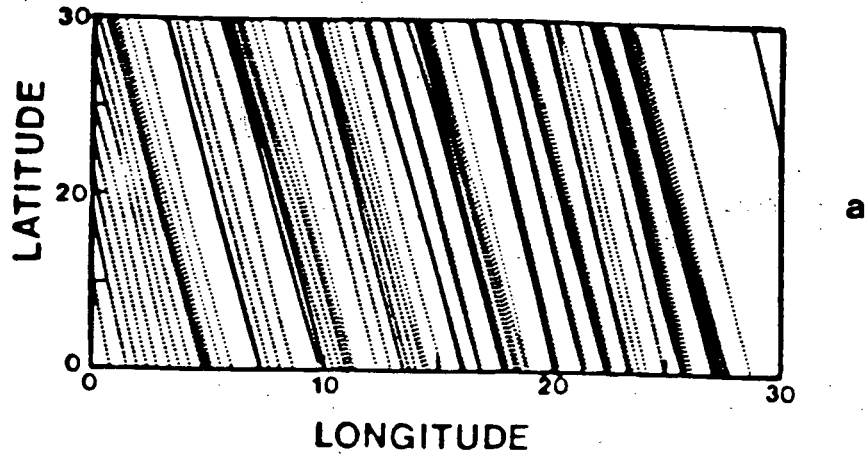
FIGURE 11. Magsat data distribution for study area with a) ascending orbits and b) descending orbits.
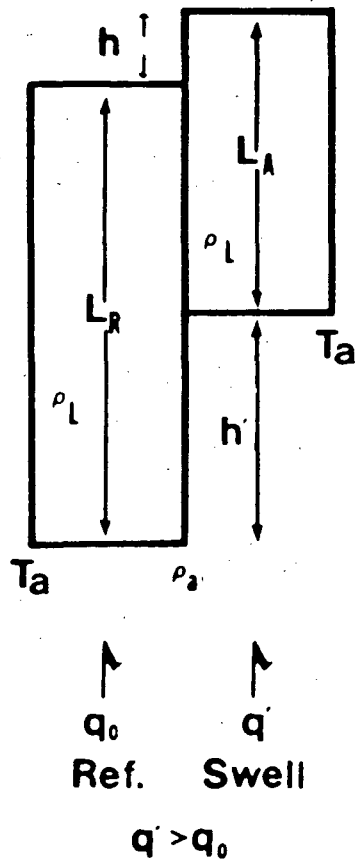
FIGURE 12. Basin and swell (or hotspot) model. Reference lithosphere is of thickness L_R. Enhanced heat flow q' (> normal, q_o) thins and isostatically uplifts the lithosphere and amount h.
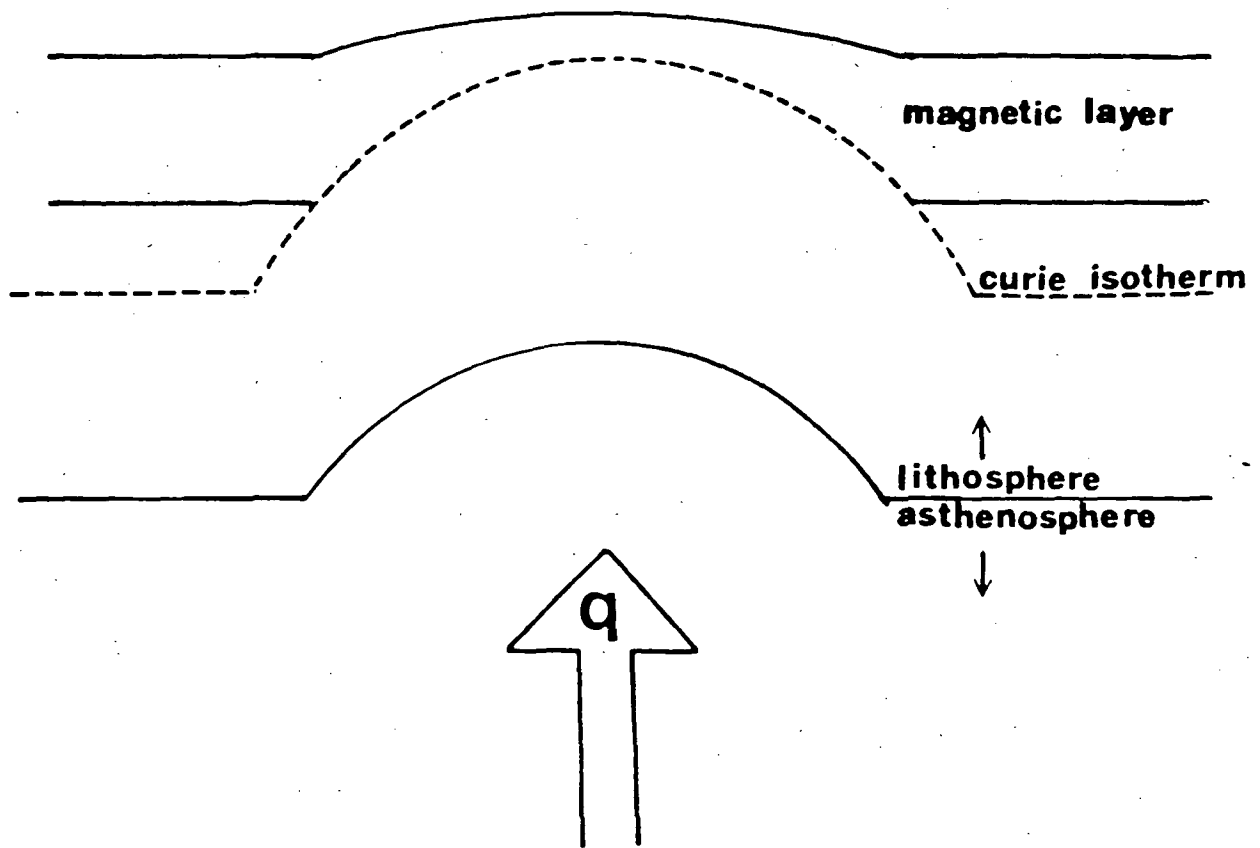
FIGURE 13. Schematic model showing how an enhanced heat flow at the base of the lithosphere raises the Curie isotherm.
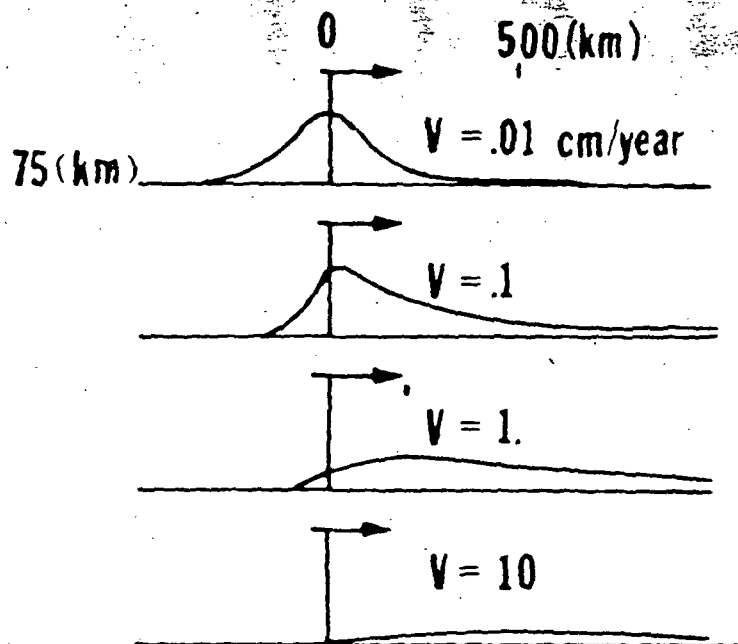
FIGURE 14. The variations in depth to the 1300° isotherm for a point source of heat at a depth of 75 kilometers with increasing plate velocity (after Birch, 1975).

CURIE SURFACE
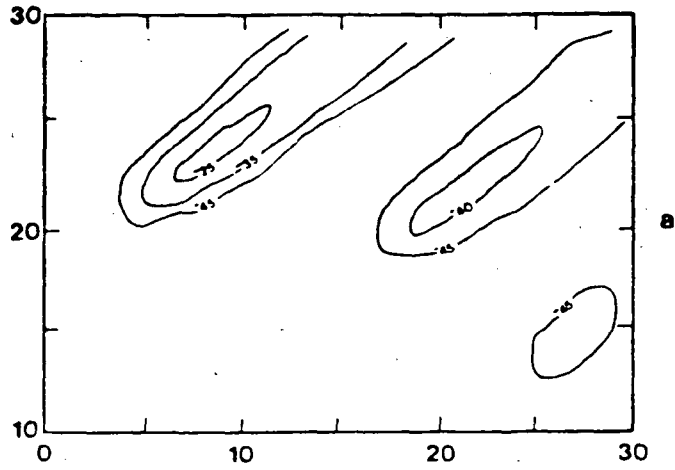
CURIE SURFACE
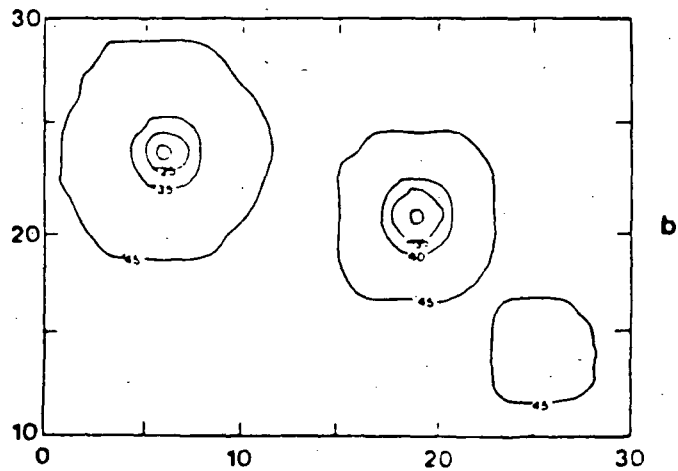
FIGURE 15. Depth to the Curie isotherm for proposed a) moving plate and b) fixed plate models (in kilometers).
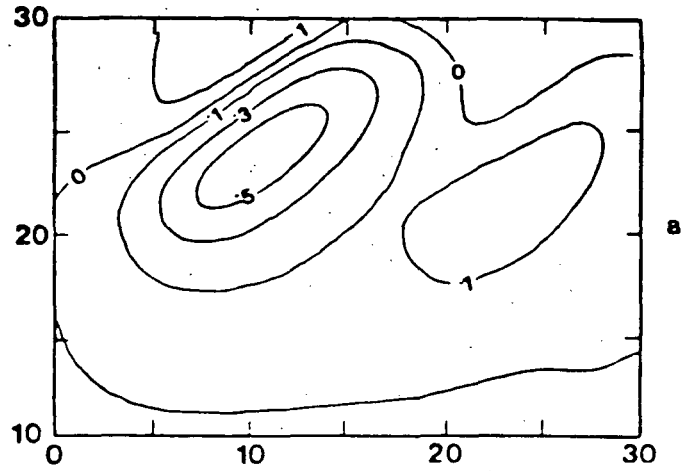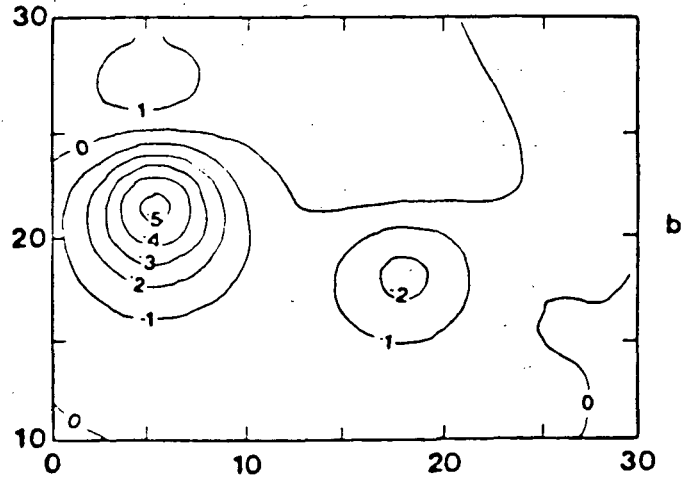
FIGURE 16. Proposed vertical component a) moving plate and b) fixed plate models (in gammas).

MOVING PLATE
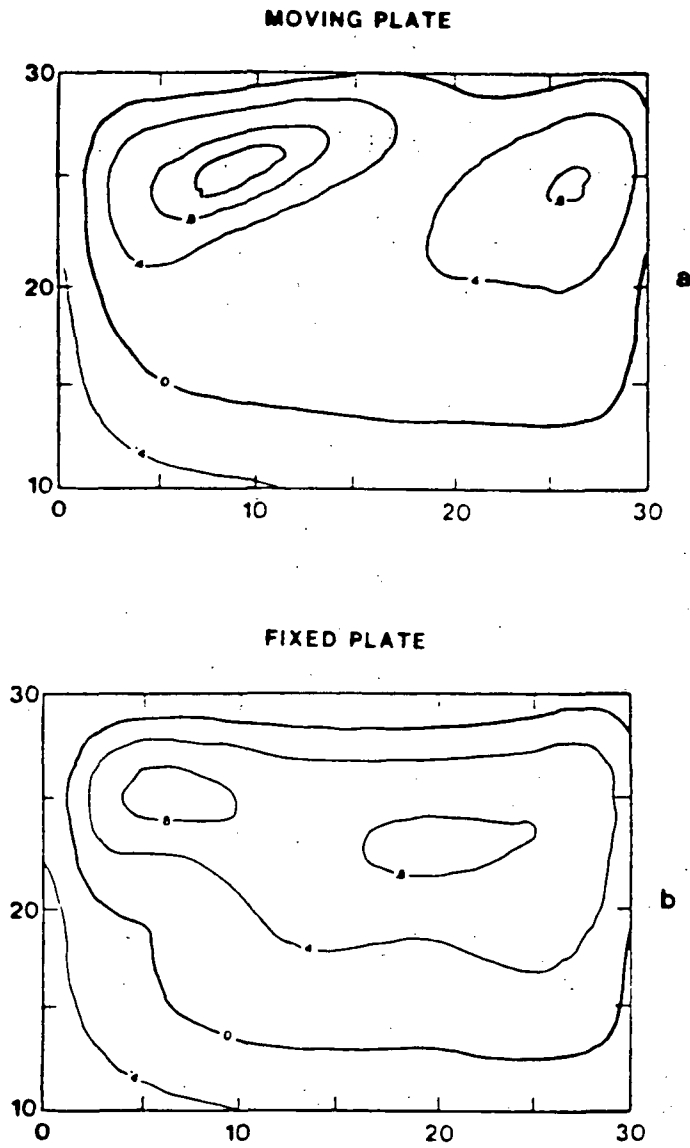
FIXED PLATE

FIGURE 17. Proposed scalar component a) moving plate and b) fixed plate models (in gammas).

VERTICAL

VERTICAL (dusk)

VERTICAL (dawn)
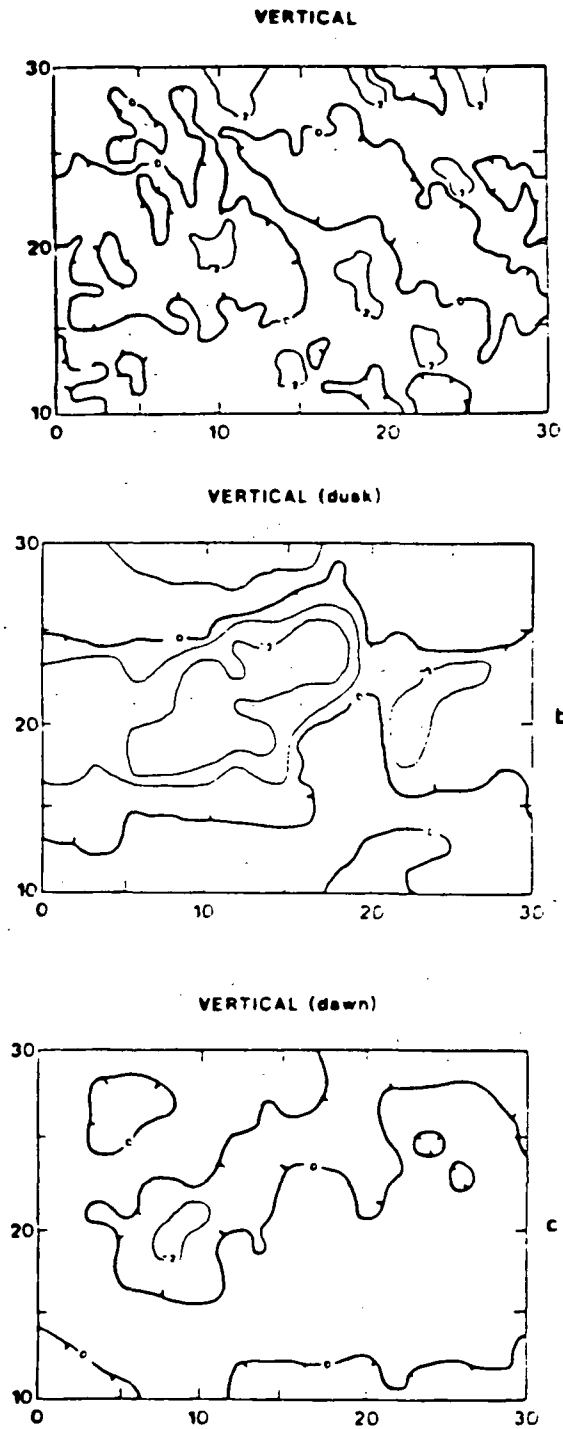
FIGURE 18. The a) vertical component map and b) ascending orbits and c) descending orbits maps (in gammas).

SCALAR

SCALAR (dusk)

SCALAR (dawn)
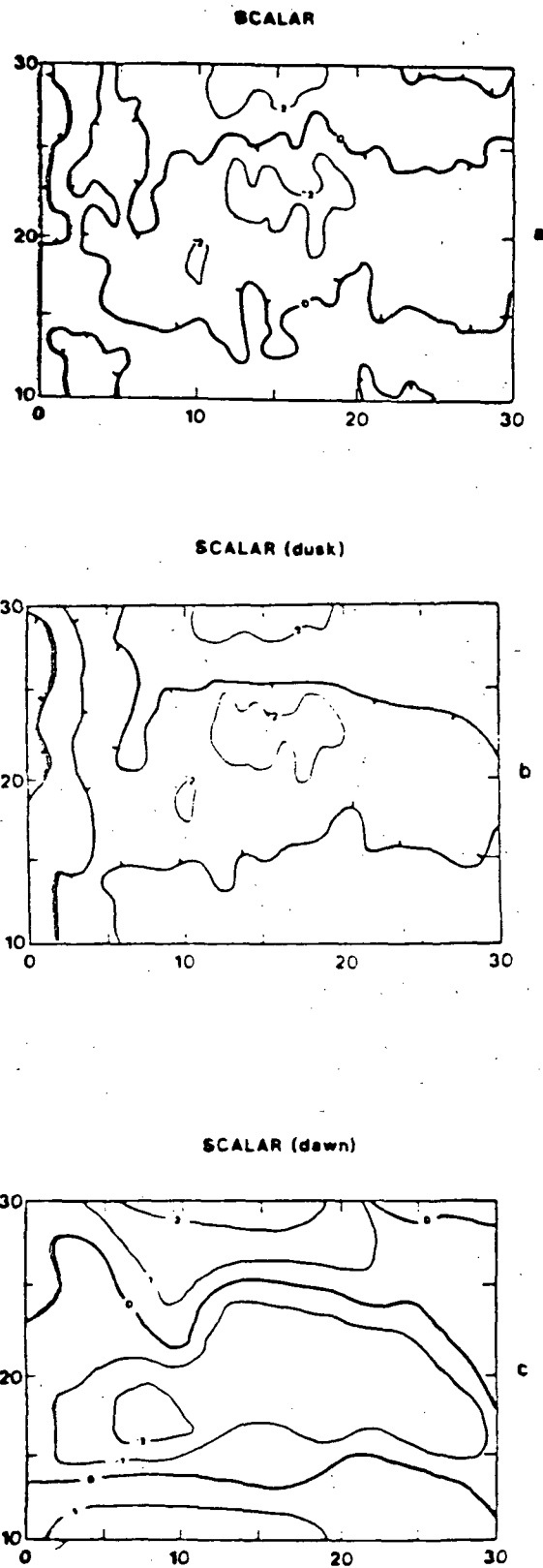
FIGURE 19. The a) scalar component map and b) ascending orbits and c) descending orbits maps (in gammas).
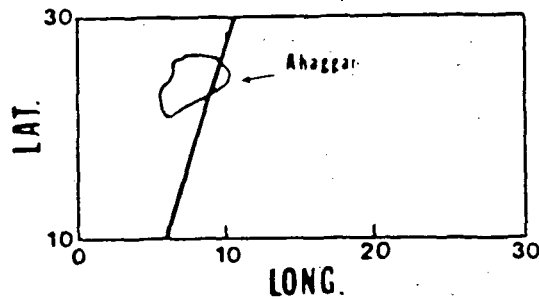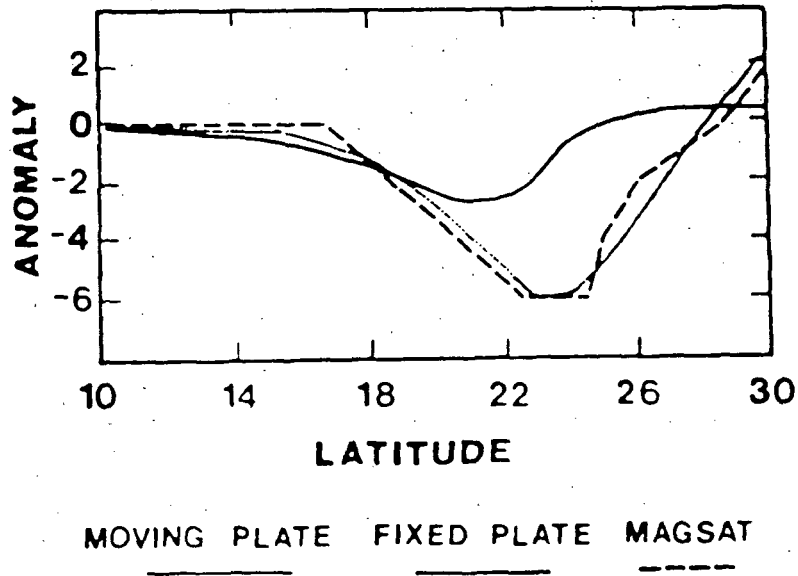
FIGURE 20. Profile across the Ahaggar uplift showing the relationship between the proposed fixed and moving plate models and the published vertical component map.
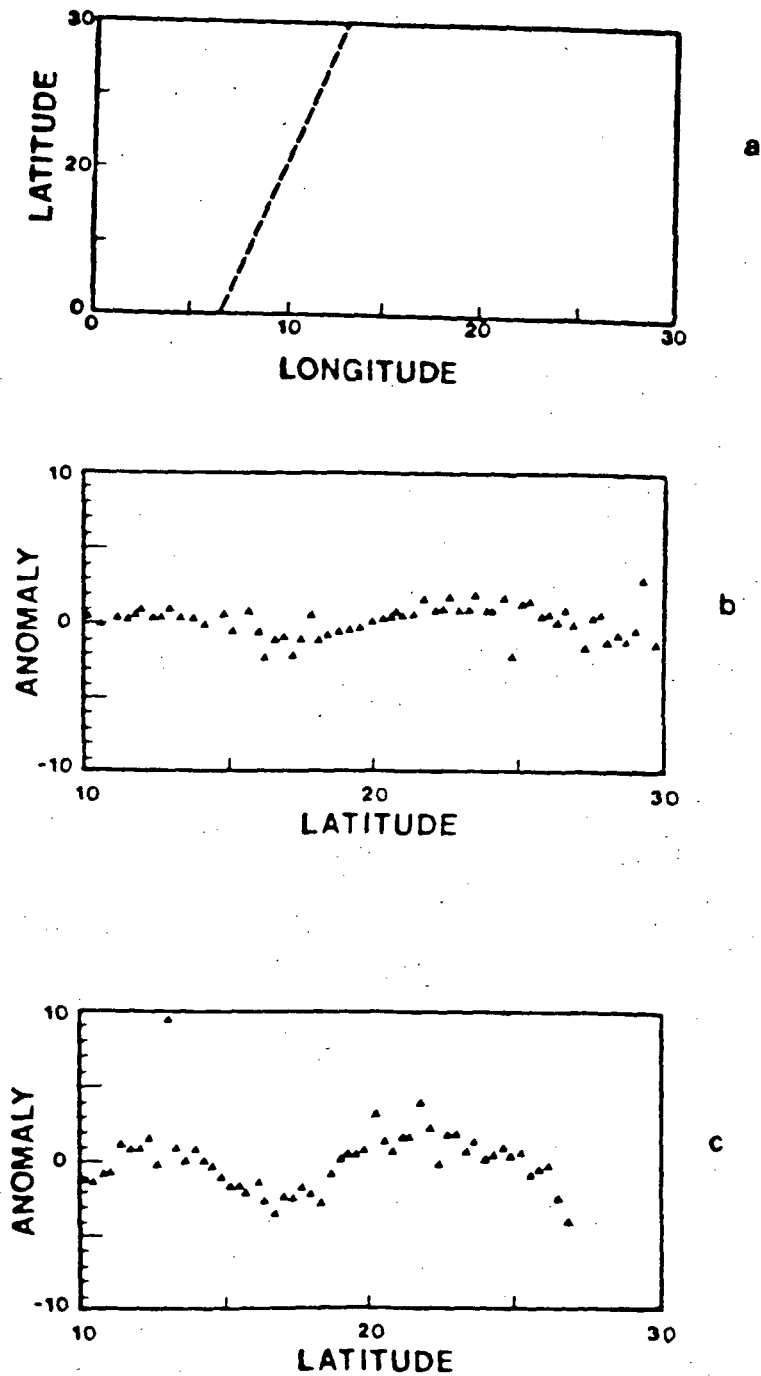
FIGURE 21. a) Latitude/longitude position of orbits 326 and 2606 and orbits b) 326 and c) 2606 after trend removal (scalar data).
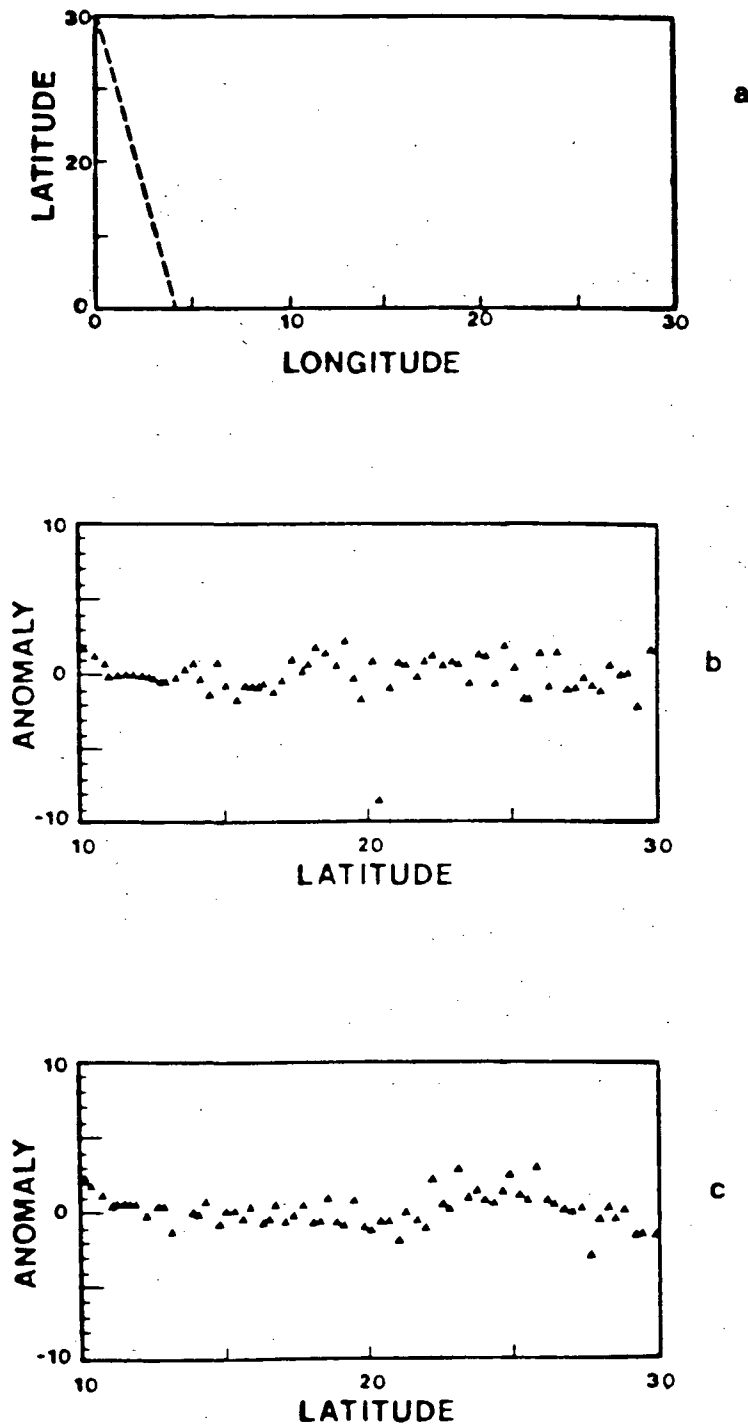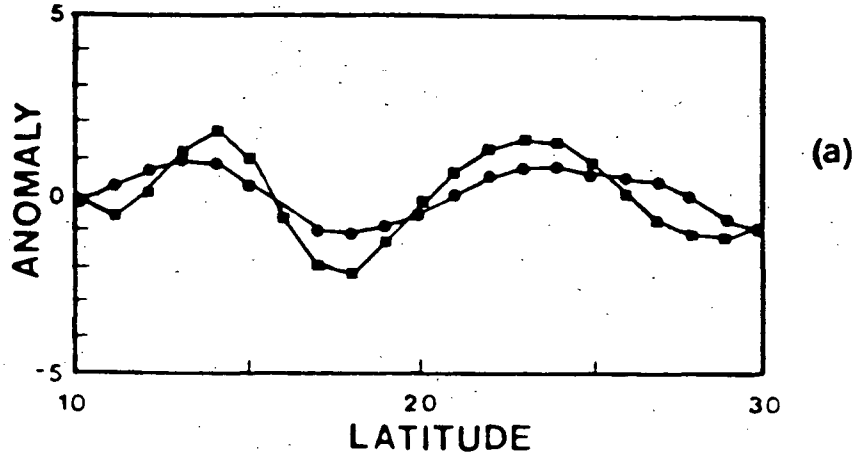
FIGURE 22. a) Latitude/longitude position of orbits 2630 and 1322 and orbits b) 2630 and c) 1322 after trend removal (scalar data).
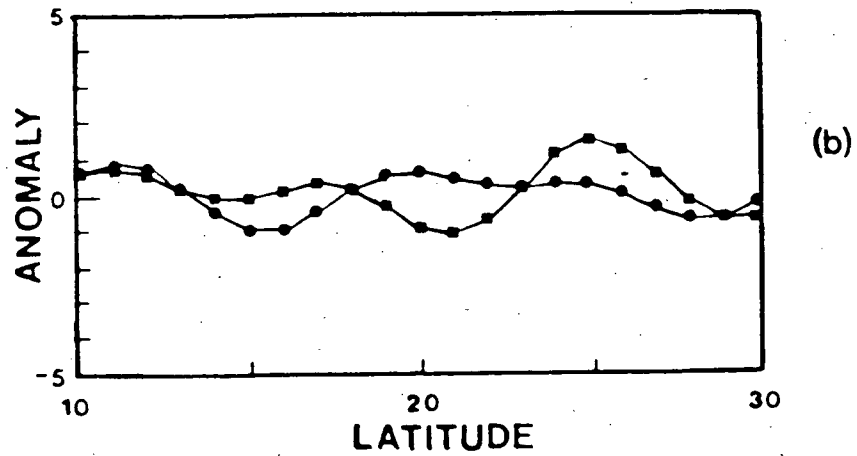
FIGURE 23. a) Descending (dawn) scalar data orbits 326 (circles) and 2602 (squares) and b) ascending (dusk) scalar orbits 2630 (circles) and 1322 (squares) after filtering.
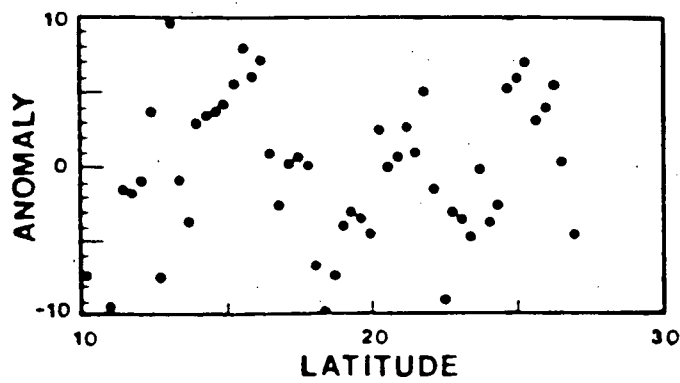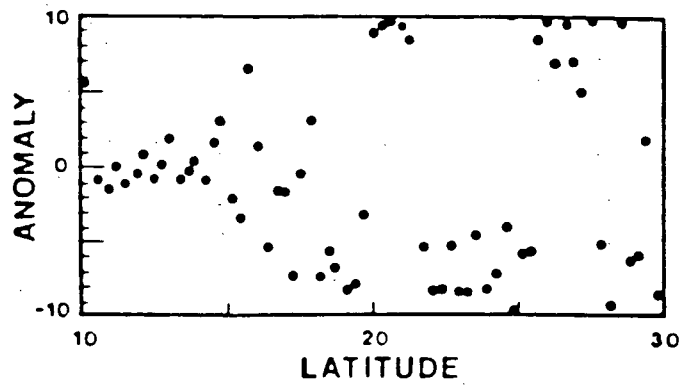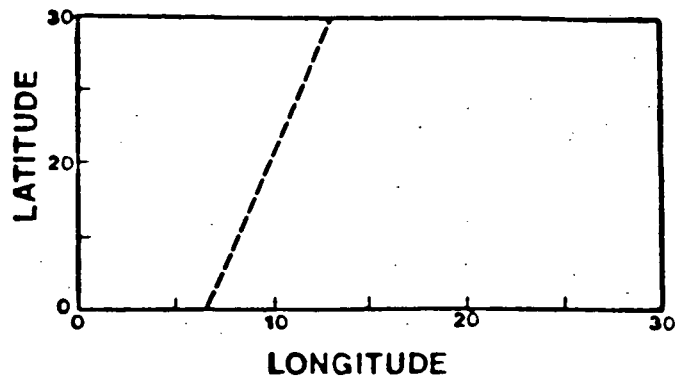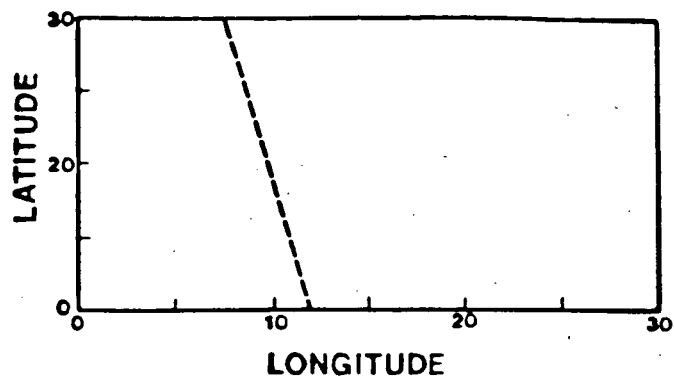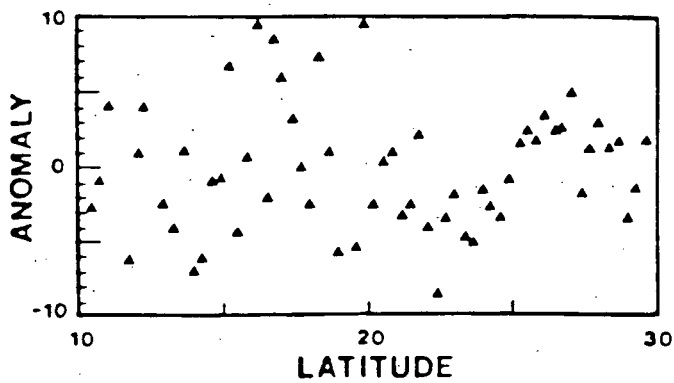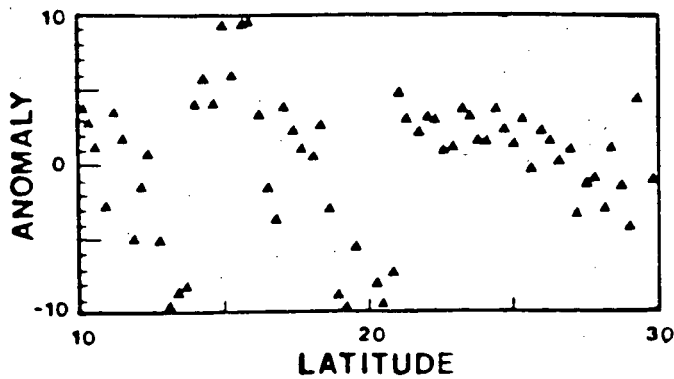
FIGURE 24. a) Latitude/longitude positioning of orbits 326 and 2606 and orbits b) 326 and c) 2606 after trend removal (vertical data).

FIGURE 25. a) Latitude/longitude position of orbits 611 and 2614 and orbits b) 611 and c) 2614 after trend removal (vertical data).
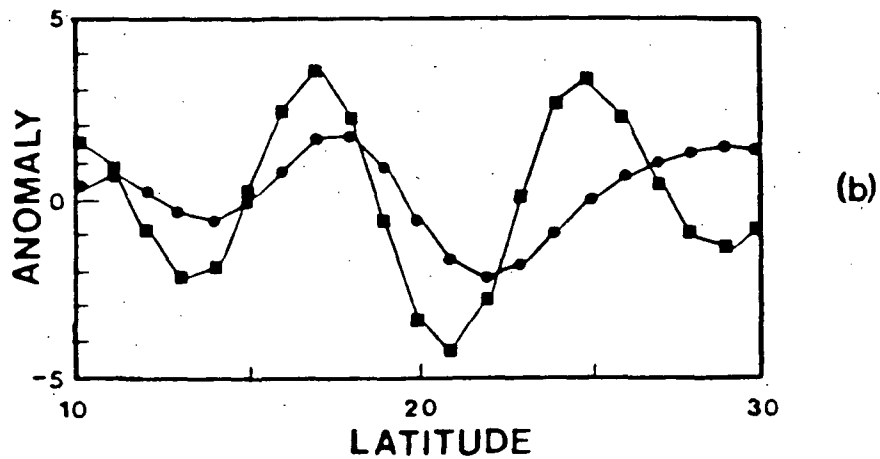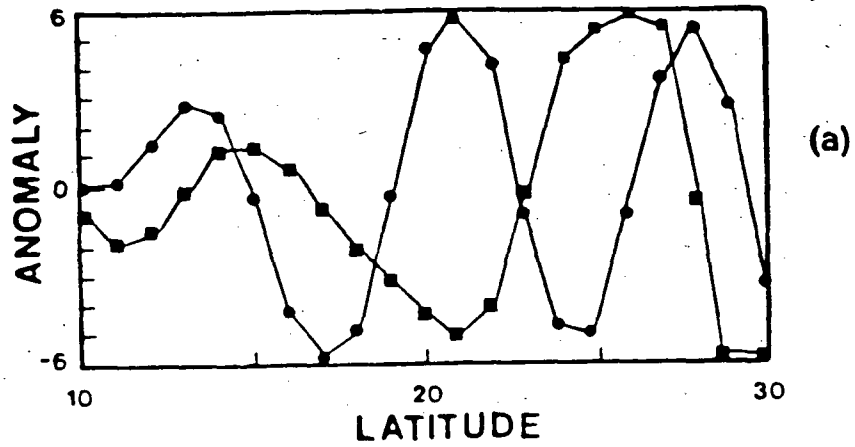
FIGURE 26. a) Descending (dawn) vertical orbits 326 (circles) and 2606 (squares) and b) ascending (dusk) orbits 611 (circles) and 2614 (squares) after filtering.
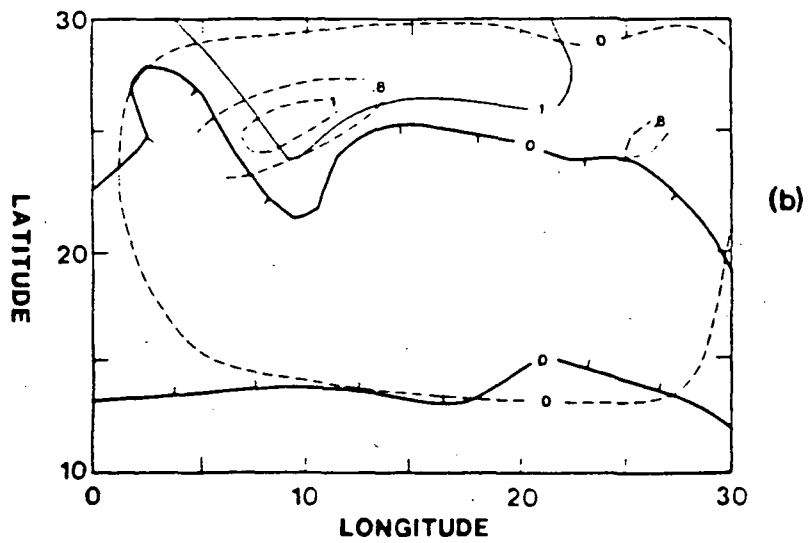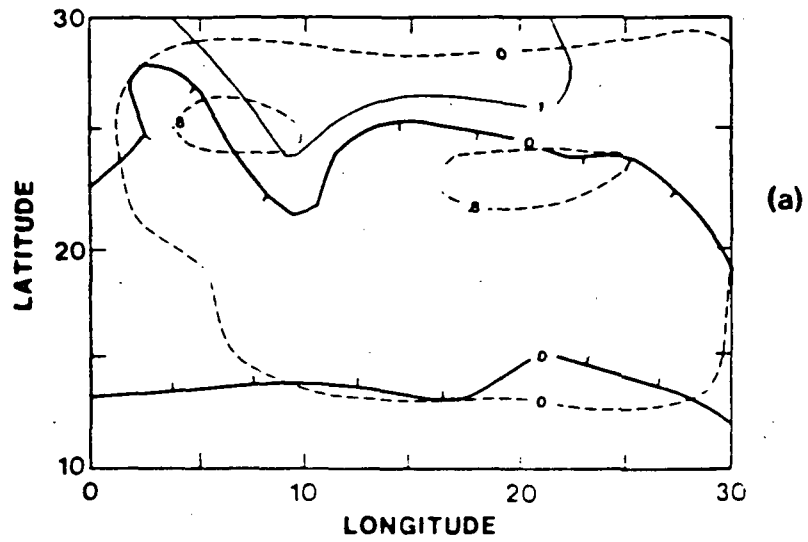
FIGURE 27. Scalar ascending orbits data (solid lines) plotted with a) fixed plate and b) moving plate models (dashed lines) (in gammas).

C - 2

TABLE 1

ERROR BUDGET

Error Source	Scalar(gammas)	Vector(gammas)
1. instrument	1.5	3.0
2. position and time	1.0	1.0
3. digitization	0.5	0.5
4. attitude error (20" @50,000)	-	4.8
5. spacecraft fields	0.5	0.5
	-------	-------
r.s.s	1.96	5.8

(after Langel et al. 1982c)

TABLE 2

MODEL PARAMETERS

Fixed Plate Model

	Source Strength (cal/sec)	Source Depth (kilometers)
1. Ahaggar	$Q = 1 \times 10^9$	$Z = 100$
2. Tibesti	$Q = 5 \times 10^8$	$Z = 100$
3. Darfur	$Q = 1 \times 10^8$	$Z = 175$

Moving Plate Model

	Source Strength	Source Depth
1. Ahaggar	$Q = 2 \times 10^9$	$Z = 125$
2. Tibesti	$Q = 1 \times 10^9$	$Z = 125$
3. Darfur	$Q = 1 \times 10^8$	$Z = 125$

Plate Velocity $= .75$ cm/yr

Plate Direction $= 35^\circ$

Curie Temperature $= 550^\circ C$

REFERENCES

Arkani-Hamed, J. and Strangway, D. W., 1984a, An interpretation of the magnetic signatures of aulacogens and cratons in Africa and South America, (submitted to) Tectonophysics.

Arkani-Hamed, J. and Strangway, D. W., 1984b, Lateral variations of apparent magnetic susceptibility of lithosphere deduced from MAGSAT data, (submitted to) Journal of Geophysical Research.

Bermingham, P.M., Fairhead, J.D. and Stuart, G.W., 1983, Gravity study of the central African rift system: a model of continental disruption, Tectonophysics, 94, 205-222.

Birch, Francis S., 1975, Conductive heat flow anomalies over a hotspot in a moving medium, Journal of Geophysical Research, 80, 4825-4827.

Black, R, and Girod, M., 1970, Late Paleozoic to Recent igneous activity in West Africa and its relationship to basement structures, in African Magmatism and Tectonics, ed. Clifford, T.N. and Gass, I.G., Hafner Pub. Co., Conneticut, 185-210.

Briden, J.C. and Gass, I.G., 1974, Plate movement and continental magmatism, Nature, 248, 650-653, 1974.

Brown, C., Girdler, R.W. and Renner, R.G.B., 1980, A gravity traverse across Northern Africa, Journal of Geophysical Research, 85, 6436-6442.

Brown, C. and Girdler, R.W., 1980, Interpretation of African gravity and its implication for the breakup of the continents, Journal of Geophysical Research, 85, 6443-6455.

Browne, S.E. and Fairhead, J.D.,1983,Gravity study of the central African rift system: a model for continental disruption 1. the Ngaoundere and Abu Gabra rifts, Tectonophysics, 94, 187-203.

Burke, K. and Dewey, J.F., 1974, Two plates in Africa during the Cretaceous ?, Nature, 249, 313-316.

Burke, K., Kidd, W.S.F. and Wilson, J. Tuzo, 1973, Relative and latitudinal motion of Atlantic hot spots, Nature, 245, 133-137.

Burke, K. and Wilson, J.T., 1972, Is the African plate stationary?, Nature, 239, 387-389.

Chase, Clement G., 1978, Plate kinematics: the Americas, East Africa, and the rest of the world, Earth and Planetary Science Letters, 37, 355-368.

Coney, Peter J., 1977, Mesozoic and Cenozoic Cordilleran plate tectonics, Geological Society of America Memoir 152, 33-50.

Crough, S. Thomas, 1981a, The Darfur swell, Africa: gravity constraints on its isostatic compensation, Geophys. Res. Let., 8, 877-879.

Crough, S. Thomas, 1981b, Free-air gravity over the Hoggar Massif, northwest Africa: evidence for the alteration of the lithosphere, Tectonophysics, 77, 189-202.

Crough, S. Thomas, 1979, Hotspot epeirogeny, Tectonophysics, 61, 321-333.

Crough, S. Thomas, 1978, Thermal origin of mid-plate hotspot swells, Geophys. J. R. astr. Soc., 55, 452-469.

Duncan, R.A., 1981, Hotspots in the southern oceans-an absolute frame of reference for motion of the Gondwana continents, Tectonophysics, 74, 29-42.

Fairhead, J.D., 1980, The intra-plate volcanic centres of North Africa and their possible relation to the East African rift system, Atti dei Convengni Zincei, 47-48.

Fairhead, J.D., 1979, A gravity link between the domally uplifted Cainozoic volcanic centres of North Africa and its similarities to the East African rift system anomaly, Earth and Planetary Science Letters, 42, 109-113.

Fairhead, J.D. and Girdler, R.W., 1971, The seismicity of Africa, Geophys. J. R. astr. Soc., 24, 271-301.

Fairhead, J.D. and Reeves, C.V., 1977, Teleseismic delay times, anomalies and inferred thickness of the African lithosphere, Earth and Planetary Science Letters, 36 63-76.

Francis, P.W., Thorpe, R.S. and Ahmed, F., 1973, Setting and significance of Tertiary to Recent volcanism in the Darfur province of Western Sudan, Nature Physical Science, 243, 30-32.

Galliher, S.C. and Mayhew, M.A., 1982, On the possibility of detecting large-scale crustal remanent magnetization with MAGSAT vector anomaly data, Geophysical Research Letters, 9, 325-328.

Gass, I.G., Chapman, D.S., Pollack, H.N. and Thorpe, R.S, 1978, Geologic and geophysical parameters of mid-plate volcanism, Phil. Trans. Soc. Lond. A, 288, 581-597.

Girdler, R.W. and Styles, P., 1974, Two stage Red Sea floor spreading, Nature, 247, 7-10.

Haggerty, Stephen E., 1978, Mineralogical constraints on Curie isotherms in deep crustal magnetic anomalies, Geophysical Research Letters, 5, 105-108.

Hastings, David A., 1982, Preliminary correlations of MAGSAT anomalies with tectonic features in Africa, Geophysical Research Letters, 9, 303-306.

Jain, Birendra K. and Regan, Robert D., 1982, Integration of satellite and conventional geophysical data with tectonic and structural information over the African continent, Geoexploration, 20, 233-258.

LaBrecque, J.L. and Cande, S.C., 1984, Intermediate wavelength magnetic anomalies over the central Pacific, Journal of Geophysical Research , 89, B13, 11124-11134.

Langel, R.A., 1982, The magnetic earth as seen from MAGSAT, initial results, Geophysical Research Letters, 9, 239-242.

Langel, R.A. and Estes, R.H., 1982, A geomagnetic field spectrum, Geophysical Research Letters, 9, 250-253.

Langel, R.A., Phillips, J.D. and Horner, R.J., 1982a, Initial scalar magnetic anomaly map from MAGSAT, Geophysical Research Letters, 9, 269-272.

Langel, R.A., Schnetzler, C.C., Phillips, J.D. and Horner, R.J., 1982b, Initial vector magnetic anomaly map from MAGSAT, Geophysical Research Letters, 9, 273-298.

Langel, R.A., Ousley, Gilbert, Berbert, John, Murphy, James and Settle, Mark, 1982c, The MAGSAT mission, Geophysical Research Letters, 9, 243-245.

Maeda, H., Iyemori, T., Araki, T. and Kamei, T., 1982, New evidence of a meridional current system in the

equatorial ionosphere, Geophysical Research Letters, 9, 337-340.

McKenzie, Dan and Sclater, John G., 1971, The evolution of the Indian Ocean since the late Cretaceous, Geophys. J. R. astr. Soc., 25, 437-528.

Morgan, J.W., 1972, Deep mantle convection plumes and plate motion, American Association of Petroleum Geologists Bulletin, 56, 203-213.

Parker, R.L., 1972, The rapid calculation of potential anomalies, Geophys. J. R. astr. Soc., 31, 447-455.

Regan Robert D. and Marsh, Bruce D., 1982, The Bangui magnetic anomaly: its geological origin, Journal of Geophysical Research, 87, 1107-1120.

Sailor, R.V., Lazarewicz, A.R. and Brammer, R.F., 1982, Spatial resolution of MAGSAT crustal anomaly data over the Indian Ocean, Geophysical Research Letters, 9, 289-292.

Vail, J.R., 1970, Tectonic control of dykes and related erruptive rocks in Eastern Africa, in African Magmatism and Tectonics, ed. Clifford, T.N. and Gass, I.G., Hafner Pub. Co., Conneticut, 337-354.

Vincent, P.M., 1970, The evolution of Tibesti volcanic province, Eastern Sahara, in African Magmatism and and Tectonics, ed. Clifford, T.N. and Gass, I.G., Hafner Pub. Co., Conneticut, 301-320.

Wasilewski, Peter J., Thomas, Herman H. and Mayhew, M.A., 1979, The MOHO as a magnetic boundary, Geophysical Research Letters, 6, 541-544.

Wilson, J. T., 1963, Continental drift, Sci. Am., 208, 86-100.

Yee-han Ng, Carolyn, 1983, Combined use of wavenumber analysis of Landsat digital imagery and seismic data to infer the orientation of tectonic stress in the Hoggar region of Africa, Master of Science Thesis, Pennslyvania State Univ., 120p.